doi.org/10.26434/chemrxiv.8411408.v1

Escherichia Coli FeoC Binds a Redox-Active, Rapidly Oxygen-Sensitive [4Fe-4S] Cluster

Aaron T. Smith, Richard O. Linkous, Nathan J. Max, Alexandrea E. Sestok, Veronika A. Szalai, Kelly N. Chacón

Submitted date: 01/07/2019 • Posted date: 02/07/2019

Citation information: Smith, Aaron T.; Linkous, Richard O.; Max, Nathan J.; Sestok, Alexandrea E.; Szalai, Veronika A.; Chacón, Kelly N. (2019): Escherichia Coli FeoC Binds a Redox-Active, Rapidly Oxygen-Sensitive [4Fe-4S] Cluster. ChemRxiv. Preprint.

The acquisition of iron is essential to establishing virulence among most pathogens. Under acidic and/or anaerobic conditions, most bacteria utilize the widely-distributed ferrous iron (Fe^{2+}) uptake (Feo) system to import metabolically-required iron. The Feo system is inadequately understood at the atomic, molecular, and mechanistic levels, but we do know it is comprised of a main membrane component (FeoB) essential for iron translocation, as well as two small, cytosolic proteins (FeoA and FeoC) hypothesized to function as accessories to this process. FeoC has many hypothetical functions, including that of an iron-responsive transcriptional regulator. Here, we demonstrate for the first time that Escherichia coli FeoC (EcFeoC) binds an [Fe-S] cluster. Using electronic absorption, X-ray absorption, and electron paramagnetic resonance spectroscopies, we extensively characterize the nature of this cluster. Under strictly anaerobic conditions after chemical reconstitution, we demonstrate that EcFeoC binds a redox-active $[4Fe\text{-}4S]^{2+/+}$cluster that is rapidly oxygen-sensitive ($t_{½}$≈ 20 s), similar to the [Fe-S] cluster in the fumarate and nitrate reductase (FNR) transcriptional regulator. In a manner similar to FNR, we further probed the nature of the oxygen-induced cluster decay products and report conversion of a $[4Fe\text{-}4S]^{2+}$cluster to a $[2Fe\text{-}2S]^{2+}$cluster. In contrast to FNR, we show that $[4Fe\text{-}4S]^{2+}$cluster binding to EcFeoC is associated with modest conformational changes of the polypeptide, but not protein dimerization. Finally, we posit a working hypothesis in which the cluster-binding FeoCs may function as oxygen-sensitive iron sensors that fine-tune pathogenic ferrous iron acquisition.

File list (2)

Escherichia coli FeoC binds a redox-active, rapidly oxygen-sensitive [4Fe-4S] cluster

Aaron T. Smith[1]✉, Richard O. Linkous[1], Nathan J. Max[1], Alexandrea E. Sestok[1], Veronika A. Szalai[2], and Kelly N. Chacón[3]

[1]Department of Chemistry and Biochemistry, University of Maryland, Baltimore County, Baltimore, Maryland, 21250 USA

[2]Physical Measurement Laboratory, National Institute of Standards and Technology, Gaithersburg, Maryland, 20899, USA

[3]Department of Chemistry, Reed College, Portland, OR, 97202, USA

✉To whom correspondence should be addressed. Tel: 410-455-1985; E-mail: smitha@umbc.edu

Abstract

The acquisition of iron is essential to establishing virulence among most pathogens. Under acidic and/or anaerobic conditions, most bacteria utilize the widely-distributed ferrous iron (Fe^{2+}) uptake (Feo) system to import metabolically-required iron. The Feo system is inadequately understood at the atomic, molecular, and mechanistic levels, but we do know it is comprised of a main membrane component (FeoB) essential for iron translocation, as well as two small, cytosolic proteins (FeoA and FeoC) hypothesized to function as accessories to this process. FeoC has many hypothetical functions, including that of an iron-responsive transcriptional regulator. Here, we demonstrate for the first time that *Escherichia coli* FeoC (*Ec*FeoC) binds an [Fe-S] cluster. Using electronic absorption, X-ray absorption, and electron paramagnetic resonance spectroscopies, we extensively characterize the nature of this cluster. Under strictly anaerobic conditions after chemical reconstitution, we demonstrate that *Ec*FeoC binds a redox-active $[4Fe\text{-}4S]^{2+/+}$ cluster that is rapidly oxygen-sensitive ($t_{½} \approx 20$ s), similar to the [Fe-S] cluster in the fumarate and nitrate reductase (FNR) transcriptional regulator. In a manner similar to FNR, we further probed the nature of the oxygen-induced cluster decay products and report conversion of a $[4Fe\text{-}4S]^{2+}$ cluster to a $[2Fe\text{-}2S]^{2+}$ cluster. In contrast to FNR, we show that $[4Fe\text{-}4S]^{2+}$ cluster binding to *Ec*FeoC is associated with modest conformational changes of the polypeptide, but not protein dimerization. Finally, we posit a working hypothesis in which the cluster-binding FeoCs may function as oxygen-sensitive iron sensors that fine-tune pathogenic ferrous iron acquisition.

Abbreviations

CD, circular dichroism; DLS, dynamic light scattering; DTT, dithiothreitol; EPR, electron paramagnetic resonance; EXAFS, extended X-ray absorption fine structure; FNR, fumarate and nitrate reductase; FUR, ferric uptake regulator; GDP, guanosine diphosphate; GTP, guanosine triphosphate; HiPIP, high potential iron-sulfur protein; HTH, helix-turn-helix; MBP, maltose-binding protein; MOPS, 3-(*N*-morpholino)propanesulfonic acid; NFeoB, soluble N-terminal GTP-binding domain of FeoB; SDS-PAGE, sodium dodecyl sulfate polyacrylamide gel electrophoresis; SEC, size-exclusion chromatography; TEV, Tobacco Etch Virus; Tris, tris(hydroxymethyl)aminomethane; TCEP, tris(2-carboxyethyl)phosphine; XAS, X-ray absorption spectroscopy.

Introduction

Iron is an essential element in numerous indispensable biological processes thus necessitating its availability for the survival of virtually every organism.[1-3] For disease-causing bacteria such as the Gram-negative pathogen *Escherichia coli*, the acquisition of iron is an essential virulence factor for the establishment of infection.[4-6] During this process, the source of bacterial iron is typically the host, where it may be found in multiple oxidation and/or coordination states, necessitating pathogens to adapt to acquire iron in ferric (Fe^{3+}), ferrous (Fe^{2+}), and even chelated forms.[5-7] Under oxidizing conditions, siderophore- and heme-based acquisition systems are essential to stabilize, to solubilize, and to transport ferric iron, whereas under acidic, micro-aerobic, and/or anaerobic conditions, such as those found in the gut or within biofilms, iron may be prevalent and soluble in the reduced, ferrous form.[7] Because each oxidation state of iron has differences in coordination geometries, ligand preferences, and even ion lability, bacteria such as *E. coli* must maintain multiple transport systems to handle these various forms of this vital element.

The ferrous iron transport system, also known as Feo, is the predominant prokaryotic Fe^{2+} transport pathway. This system is found along the *feo* operon (Fig. 1A), which was first discovered in *E. coli*.[7-9] In many bacteria, upstream of the *feo* operon are two transcriptional regulators: the ferric uptake regulator (FUR), a global iron regulator controlling transcription of numerous genes involved in iron utilization and metabolism; and the fumarate and nitrate reductase (FNR) regulator, a global iron-based regulator controlling transcription of genes involved in processes linked to anaerobic metabolism.[9-10] Downstream of these transcriptional regulators in *E. coli* are encoding regions for three proteins (Fig. 1A): FeoA, a small, cytosolic β-barrel protein thought to be an integral regulatory element; FeoB, a large polytopic membrane

protein bearing a N-terminal GTP-binding domain that moves ferrous iron across the membrane; and FeoC, a small, cytosolic winged-helix protein with an unknown function. In a Gram-negative bacterium such as *E. coli*, these three proteins are thought to function in concert to regulate the movement of ferrous iron into the cytosol to be incorporated into the intracellular labile iron pool (Fig. 1B).[7]

Although ferric siderophore- and heme-transport systems have been historically recognized as important contributors to bacterial virulence,[11-13] emerging evidence demonstrates that ferrous iron contributes significantly to the establishment of infection by a wide array of pathogens within mammalian hosts. For example, FeoA and FeoB knockouts in model pathogens have decreased or abrogated growth of several strains.[14-18] Additionally, gene knockouts of the *feo* operon native to several human pathogens have either reduced[19-20] or wholly prevented[4] colonization of these bacteria within mouse,[4] chicken,[21] and/or piglet models,[21] emphasizing the importance of this uptake pathway to bacterial infection within mammals and birds. Organisms whose normal iron homeostasis appear to be dependent either in part or wholly on the Feo system include several acute, and multiple emergent pathogens, such as *Campylobacter jejuni,*[21] *E. coli,*[22] *Francisella tularensis,*[23] *Helicobacter pylori,*[4] *Porphyromonas gingivalis,*[15-16] *Shigella flexneri,*[24] *Vibrio cholerae,*[25] and even *Yersinia pestis,*[26] underscoring the importance of ferrous iron uptake to several disease-causing bacteria. A definitive consensus regarding the contribution of Feo towards virulence and growth of the opportunistic pathogen *Pseudomonas aeruginosa* remains somewhat controversial.[27-28] However, recent findings have indicated substantive concentrations of ferrous iron (≈ 40 μmol/L) within the sputum of patients suffering from cystic fibrosis,[29] and iron availability is strongly linked to *P. aeruginosa* biofilm formation,[30-31] disease progression, and disease severity.[29] Thus it is clear that Feo-mediated ferrous iron uptake

contributes significantly to bacterial virulence, and a greater structural and mechanistic understanding of this system could allow for the rational targeting of Feo for antibacterial developments.

To this end, we sought to biochemically, biophysically, and spectroscopically characterize the FeoC component of unknown function from the Gram-negative pathogen *E. coli* (*Ec*FeoC). A bioinformatics analysis has suggested that FeoCs are found in approximately 15% of all *feo* operons but appear to be strictly limited to γ-proteobacteria.[32] NMR structures of intact *E. coli* (Fig. 1C; PDB ID 1XN7) and *Klebsiella pneumoniae* FeoC (*Kp*FeoC; PDB ID 2K02)[33] reveal an overall fold consisting of a LysR-like winged-helix motif, implicating these proteins as potential transcriptional regulators. Within the disordered "wing" of these structures are 4 Cys residues (Fig. 1C) that are strongly conserved[34] and speculated to bind an [Fe-S] cluster, which could structure this region to drive function. In support of this hypothesis, a study of recombinant *Kp*FeoC demonstrated the presence of an [Fe-S] cluster bound to this protein in low yield under aerobic conditions;[34] however, this work assigned the *Kp*FeoC cluster to an unusual $[4Fe\text{-}4S]^{3+}$ high potential iron-sulfur protein (HiPIP)-like state that was exceptionally oxygen-tolerant, leading us to question the validity of this assignment. In this work, we are the first to demonstrate that *Ec*FeoC binds an [Fe-S] cluster, and we spectroscopically and biophysically characterize the nature of this cluster. Under strictly anaerobic conditions, we demonstrate that *Ec*FeoC binds a redox-active and rapidly oxygen-sensitive $[4Fe\text{-}4S]^{2+/+}$ cluster, in distinct contrast to studies of *Kp*FeoC. Importantly, we show that this cluster binding is associated with modest conformational changes of the polypeptide but not protein dimerization, and we speculate how this cluster binding and conformational change may relate to the function of FeoC.

Materials and Methods

Materials. All materials used for buffer preparation, protein expression, and protein purification were purchased from standard commercial suppliers and were used as received. Where indicated, values are reported as the mean ± one standard deviation. Note that certain commercial equipment, instruments, or materials are identified in this paper to specify the experimental procedure adequately. Such identification is not intended to imply recommendation or endorsement by the National Institute of Standards and Technology, nor is it intended to imply that the materials or equipment identified are necessarily the best available for the purpose.

Cloning, Expression, Purification, and Cleavage of EcFeoC. DNA encoding for the gene corresponding to FeoC from *Escherichia coli* (strain K12) (Uniprot identifier P64638) (*Ec*FeoC) was commercially synthesized by GenScript (Piscataway, NJ), with an additionally engineered DNA sequence encoding for a C-terminal TEV-protease cleavage site (ENLYFQG) or with an additionally engineered DNA sequence encoding for an N-terminal maltose-binding protein sequence (based on P0AEX9: *Escherichia coli* (K12) *malE* gene product) followed by a Tobacco Etch Virus (TEV)-protease cleavage site. The former gene was subcloned into the pET-21a(+) expression plasmid using the NdeI and XhoI restriction sites, encoding for a C-terminal $(His)_6$ affinity tag when read in-frame. The latter gene was subcloned into the pET-45b(+) expression plasmid using the PmlI and PacI restriction sites, encoding for a N-terminal $(His)_6$ affinity tag followed by maltose-binding protein when read in-frame.

The complete expression plasmid was transformed into chemically competent BL21(DE3) cells, spread onto Luria-Bertani (LB) agar plates supplemented with 100 μg/mL ampicillin (final concentration), and grown overnight at 37 °C. Colonies from these plates served as the source of *E. coli* for small-scale starter cultures (generally 100 mL LB supplemented with

100 μg/mL ampicillin as a final concentration). Large-scale expression of each construct was accomplished in 12 baffled flasks each containing 1 L sterile LB supplemented with 100 μg/mL (final concentration) ampicillin and inoculated with a pre-culture. Cells were grown by incubating these flasks at 37 °C with shaking until the optical density at 600 nm (OD_{600}) was approximately 0.6 to 0.8. The flasks containing cells and media were then chilled to 4 °C for 2 h, after which protein expression was induced by the addition of isopropyl β-D-l-thiogalactopyranoside (IPTG) to a final concentration of 1 mmol/L The temperature of the incubator shaker was lowered to 18 °C with continued shaking at 20.9 rad/s (200 rpm). After approximately 18 h to 20 h, cells were harvested by centrifugation at 4800×*g*, 10 min, 4 °C. Cell pellets were subsequently resuspended in resuspension buffer (50 mmol/L Tris, pH 7.5, 200 mmol/L NaCl, 0.7 mol/L glycerol (5 % (v/v)), flash-frozen on $N_{2(l)}$, and stored at -80 °C until further use.

All steps for the purification of MBP-*Ec*FeoC were performed at 4 °C unless otherwise noted. Frozen cells were thawed and stirred at room temperature until the solution was homogeneous. Solid phenylmethylsulfonyl fluoride (PMSF; ≈ 50 mg to 100 mg) was added immediately prior to cellular disruption using a Q700 ultrasonic cell disruptor. Cellular debris was cleared by ultracentrifugation at 163000×*g* for 1 h. The supernatant was then applied to two tandem 5 mL MBPTrap HP columns that had been pre-equilibrated with 5 column volumes (CVs) of wash buffer (25 mmol/L Tris, pH 7.5, 200 mmol/L NaCl, 0.7 mol/L glycerol (5% (v/v)), 1 mmol/L TCEP). The column was then washed with 20 CVs of wash buffer. Protein was then eluted by wash buffer containing 10 mmol/L maltose. Fractions were concentrated using a 15 mL Amicon 30 kg/mol (30 kDa) molecular-weight cutoff (MWCO) spin concentrator. Protein was then buffer exchanged in the same spin concentrator by repeated dilution and concentration

into TEV protease buffer (50 mmol/L Tris, pH 8.0, 200 mmol/L NaCl, 0.7 mol/L glycerol (5% (v/v)), 1 mmol/L TCEP, 0.5 mmol/L EDTA). Cleavage, which liberates native *Ec*FeoC with an additional Gly residue on its N-terminus, was accomplished by mixing ≈ 10 μg TEV protease per ≈ 1 mg of protein, followed by rocking at room temperature overnight. This sample was then applied directly to a 120 mL Superdex 75 gel filtration column that had been pre-equilibrated with 25 mmol/L Tris, pH 7.5, 100 mmol/L NaCl, 0.7 mol/L glycerol (5% (v/v)), and 1 mmol/L TCEP. The eluted fractions of monomeric *Ec*FeoC were pooled and concentrated with a 4 mL Amicon 3 kg/mol (3 kDa) MWCO spin concentrator. To verify size, additional size-exclusion experiments were performed in a similar manner but with a 24 mL Superdex 75 column calibrated with low-molecular weight protein standards (MilliporeSigma). Protein concentration was determined using the Lowry assay, and purity was assessed via SDS-PAGE (acrylamide mass fraction of 15%) and Tris-tricine SDS-PAGE (acrylamide mass fraction gradient from 10% to 20%) analyses.

Anaerobic Reconstitution. Samples were reconstituted in an anaerobic chamber (Coy Laboratory Products, Grass Lake, MI) containing a N_2/H_2 atmosphere and operating at < 7.05 mg/m^3 (5 ppm) O_2. Briefly, protein was brought into the anaerobic chamber and allowed to equilibrate with the anaerobic chamber's atmosphere overnight at 6 °C with shaking. Protein was then diluted to 100 μmol/L in reconstitution buffer comprising 50 mmol/L MOPS, pH 7.5, 100 mmol/L NaCl, 1 mmol/L DTT, 0.7 mol/L glycerol (5% (v/v)). 10 mmol/L stock $FeCl_3$ was first titrated into the apo protein until up to 6 mole equivalents had been added with 10 min shaking at 6 °C between the addition of each mole equivalent of Fe^{+3}. 10 mmol/L stock Na_2S was then titrated into the iron-bound protein in the same manner. Afterwards, protein was equilibrated with $FeCl_3$ and Na_2S for ≈ 2 h at 6 °C with shaking. Particulate matter was removed by first

centrifuging at 14000×*g* anaerobically for 10 min at 4 °C and then by filtration through a filter with a 0.22 μm pore size. Excess iron and sulfide were removed by buffer exchanging at least four times into fresh 50 mmol/L MOPS, pH 7.5, 100 mmol/L NaCl, 1 mmol/L DTT, 0.7 mol/L glycerol (5% (v/v)). Iron contents were determined as described below.

Iron Content Determination. Iron content was determined spectrophotometrically using a modified version of the ferrozine assay.[35-36] Briefly, protein was precipitated using 5 mol/L (50 % (v/v)) trichloroacetic acid (TCA). The supernatant was decanted and subsequently neutralized with saturated ammonium acetate. To this solution, excess ascorbic acid and 0.30 mmol/L ferrozine (final concentration) were added. Absorbance measurements of samples made in triplicate were taken at 562 nm. The concentration of Fe^{2+} was then determined assuming a Fe^{2+}-ferrozine complex with an extinction coefficient (ε_{562}) of ≈ 28 L $mmol^{-1}$ cm^{-1} [36] (26.98 L $mmol^{-1}$ cm^{-1} ± 0.96 L $mmol^{-1}$ cm^{-1})[35], and these data were corrected against residual iron present in buffer constituents.

Electronic Absorption and Circular Dichroism Spectroscopies. Electronic absorption spectra were recorded at room temperature on a Cary 60 UV-visible spectrophotometer (Agilent). Samples were contained within a 1 cm UV-transparent cuvette, and data were acquired from 800 nm to 250 nm with the instrument set to a spectral bandwidth of 2 nm. Absorption studies designed to follow the oxidation of reconstituted *Ec*FeoC were performed in two ways. First, anaerobically reconstituted protein was aliquoted into a UV-transparent cuvette and stoppered inside of an anaerobic chamber. Following removal from the anaerobic chamber, the stopper was removed, the cuvette was flushed with ambient atmosphere, and the oxidation process was monitored by scanning kinetics from 800 nm to 250 nm with spectra accumulated every 6 s until reactivity appeared to cease (≈ 15 min to 20 min). Second, air-saturated buffer (25 mmol/L Tris,

pH 7.5, 100 mmol/L NaCl, 0.7 mol/L glycerol (5 % (v/v)), and 1 mmol/L TCEP) was sealed inside of a container and brought into an anaerobic chamber. Buffer was mixed with protein, also contained inside of a septum-sealed cuvette, using a gastight syringe. Once again, the oxidation process was monitored by scanning kinetics from 800 nm to 250 nm with spectra accumulated every 6 s until reactivity appeared to cease (≈ 5 min). Observed kinetic data (k_{obs}) were fitted to the following equation:

$$Abs_t = Abs_\infty + \alpha e^{-kt}$$

Circular dichroism (CD) spectra were recorded on a nitrogen-flushed Jasco J710 spectropolarimeter operating at room temperature. Samples were contained within a 1.0 cm quartz cuvette, and data were acquired from 400 nm to 190 nm with the instrument set to a spectral bandwidth of 1 nm. Plotted CD data represent the average of 5 scans.

EPR Spectroscopy. Samples containing ≈ 100 μmol/L to 600 μmol/L iron (final concentration) in buffer plus 3.6 mol/L ethylene glycol (20% (v/v)) were aliquoted either aerobically or anaerobically (as warranted) into standard quartz X-band EPR tubes with a 4 mm outer diameter and flash-frozen in $N_{2(l)}$. Spectra were collected at temperatures indicated in the figure legend using a commercial EPR spectrometer system equipped with a high-sensitivity, TE-mode, CW resonator and commercial temperature-control unit. The uncertainty on the reported *g* values is 0.0005, using the manufacturer-reported field (0.08 mT) and frequency (0.00005 GHz) accuracies. The maximum, minimum and baseline-crossing points of peaks were used to determine magnetic field positions for *g* values. Calculated *g* values (from magnetic field values) agree with *g* values directly reported by the spectral analysis software provided with the commercial instrument to within 0.001.

X-ray Absorption Spectroscopy. Samples containing ≈ 0.5 mmol/L to 2 mmol/L iron (final concentration) in buffer plus 3.6 mol/L ethylene glycol (20% (v/v)) were aliquoted either aerobically or anaerobically (as warranted) into Lucite cells wrapped with Mylar tape, flash frozen in $N_{2(l)}$ and stored at −80 °C until data collection. X-ray absorption data was collected on beamlines 7-3 and 9-3 at the Stanford Synchrotron Radiation Lightsource (Menlo Park, CA) as replicates when possible. Extended X-ray absorption fine structure (EXAFS) of Fe (7210 eV) was measured using a Si 220 monochromator with crystal orientation ϕ = 90°. Samples were measured as frozen aqueous glasses in 3.6 mol/L ethylene glycol (20% (v/v)) at 15 K, and the X-ray absorbance was detected as K α fluorescence using either a 100-element (beamline 9-3) or 30-element (beamline 7-3) Canberra Ge array detector. A Z-1 metal oxide filter (Mn) and Soller slit assembly were placed in front of the detector to attenuate the elastic scatter peak. A sample-appropriate number of scans of a buffer blank were measured at the absorption edge and subtracted from the raw data to produce a flat pre-edge and eliminate residual Mn K β fluorescence of the metal oxide filter. Energy calibration was achieved by placing a Fe metal foil between the second and third ionization chamber. Data reduction and background subtraction were performed using EXAFSPAK.[37] The data from each detector channel were inspected for drop outs and glitches before being included into the final average. EXAFS simulation was carried out using the program EXCURVE 9.2 as previously described.[38-40] The quality of the fits was determined using the least-squares fitting parameter, F, which is defined as:

$$F^2 = \frac{1}{N}\sum_{i=0}^{N} k^6(\chi_i^{theory} - \chi_i^{exp})^2$$

and is referred to as the fit index (FI).

Dynamic Light Scattering Studies. Intensity, volume, and number distributions relating to the diameters of apo and [4Fe-4S]-bound *Ec*FeoC forms (assumed to be perfect spheres in solution)

were analyzed by dynamic light scattering (DLS) spectroscopy. DLS measurements were performed with a Malvern Zetasizer Nano ZS equipped with a 633 nm He–Ne laser and operating at an angle of 173°. Samples were prepared anaerobically in a septum-stoppered low-volume quartz cuvette at room temperature. Data are the average of three replicate scans performed on at least two independent protein preparations. Dispersities ($Đ$) had prep-to-prep variations but were generally in a range of ≈ 0.1 to 0.2, indicating uniform dispersity, correlating well with our size-exclusion analyses (*vide supra*).

Results

Expression and purification of EcFeoC.

Due to the small nature of *Ec*FeoC (≈ 9 kg/mol, 9 kDa), we needed to explore several methods to express and to purify this protein. Our initial approach was one in which we cloned the gene corresponding to *Ec*FeoC (Uniprot ID: P64638) into the IPTG-inducible pET-21a(+) expression plasmid with a cleavable, C-terminal $(His)_6$ tag (MW ≈ 10 kg/mol, 10 kDa). Despite exhaustive efforts to express this tagged protein, including multiple expression temperatures, times, and media, we were unable to observe appreciable accumulation of this expression construct with *E. coli* as the expression host. Therefore, we created a new expression construct encoding for a maltose-binding protein (MBP) fusion that we subcloned into the IPTG-inducible pET-45b(+) expression plasmid. This final expression construct encodes for an N-terminal $(His)_6$ tag tethered to MBP with a TEV protease site immediately preceding *Ec*FeoC (*i.e.*, H_2N-$(His)_6$-MBP-TEV-FeoC-COOH) (Fig. 2A). Expression of this construct was robust within *E. coli* under numerous conditions. We then took advantage of the MBP moiety of this construct for protein purification, and after a single round of affinity chromatography, we were able to purify our MBP-*Ec*FeoC fusion to high purity (estimated to be > 95%; Fig. 2) and excellent yields (> 100 mg/L of cell culture) (Fig. S1A).

After our initial round of purification, we isolated *Ec*FeoC from MBP by TEV protease cleavage and subsequent size-exclusion chromatography (SEC; Fig. 2B). After overnight incubation with the protease, complete cleavage of the starting protein construct was evident (Fig. S1A), yielding the nearly native *Ec*FeoC protein with a single additional Gly residue on the N-terminus. We then separated cleaved *Ec*FeoC from His-tagged MBP and TEV protease by size-exclusion chromatography (SEC) on Superdex 75 (Fig. 2B; Fig. S1B). This final step

yielded highly pure, monomeric *Ec*FeoC in good yield (Fig. 2C). To verify that our cleaved *Ec*FeoC construct was not unfolded after TEV protease treatment and MBP separation, we measured its far-UV circular dichroism (CD) spectrum, which displayed a mixture of α helices, β strands, and random coil, as expected (Fig. S2).

Aerobically isolated MBP-EcFeoC contains degradation products of a [4Fe-4S] cluster.

Despite the fact that MBP accounts for nearly 80% of the MBP-*Ec*FeoC fusion construct, and that we purified this construct aerobically, the presence of an [Fe-S] cluster was readily apparent, consistent with the hypothesis that *Ec*FeoC would bind a cluster based on its conservation of 4 Cys residues (Cys^{56}, Cys^{61}, Cys^{64} and Cys^{70}—all numbered based on native *Ec*FeoC). Aerobically-purified MBP-*Ec*FeoC expressed in unsupplemented LB medium bore a brownish-red color that became increasingly more intense during protein concentration, common to many [Fe-S] clusters. Metal analysis alone (iron content of (0.23 ± 0.02) ions per polypeptide, where the error is one standard deviation (confidence interval of 68.2%), derived from replicate experiments) was unable to assign the composition of the [Fe-S] cluster due to the presence of apo protein. However, most [Fe-S] clusters exhibit spectroscopic signatures that are indicative of the species that may be present.[41-42] The MBP-*Ec*FeoC electronic absorption spectrum (Fig. 3A; λ_{max} of 330 nm and 418 nm with broad, overlapping peaks from 500 nm to 600 nm) bears a similarity to the spectrum of *Kp*FeoC,[33] which was also shown to bind an [Fe-S] cluster; however, while the spectrum of *Kp*FeoC was previously attributed to the presence of an unusual oxygen-stable $[4Fe\text{-}4S]^{3+}$ HiPIP cluster,[33] the electronic absorption spectral signatures of both proteins are distinctly different from purely [4Fe-4S] or [2Fe-2S] clusters, potentially indicating multiple species.[43]

To probe the identity of the species in the MBP-*Ec*FeoC fusion construct, we analyzed the X-ray absorption (XAS) and electron paramagnetic resonance (EPR) spectra of this aerobically-isolated construct (Figs. 4A, 5A). Because both types of spectroscopy are sensitive to the nature, number, and types of nearest-neighbor ligands, as well as the oxidation state and number of unpaired electrons on the iron centers, these approaches can function to differentiate various cluster compositions from one another. Simulations of the extended X-ray absorption fine structure (EXAFS) data of MBP-*Ec*FeoC taken at the Fe edge reveal only S-based environments as the nearest neighbor ligands with an average distance of 0.226 nm ± 0.005 nm (2.26 Å ± 0.05 Å) (Fig. 4A and inset; Table 1), consistent with the presence of an [Fe-S] cluster. The involvement of any Cys residues must come from the *Ec*FeoC moiety, as there are no other Cys residues within the fusion construct, and the average Fe-S interactions are best fitted with a coordination number of 3. There is no indication of O/N-nearest neighbor ligands, precluding the involvement of the His tag in Fe binding. Furthermore, the presence of a higher-order cluster is suggested, as long-range scattering interactions of an Fe-Fe vector are observed and fitted to a distance of 0.272 nm ± 0.005 nm (2.72 Å ± 0.05 Å) (Fig. 4A, Table 1). To probe the [Fe-S] compositions further, continuous wave (CW) X-band EPR spectroscopy was used, which indicates an admixture of different clusters. When analyzed over a range of 400 mT, the as-isolated, aerobic form of MBP-*Ec*FeoC has a single, strong EPR signal at $g \approx 4.3$ (Fig. 5A) at multiple temperatures, almost identical to the signal seen in oxidized rubredoxins[44] (*i.e.*, $[Fe^{3+}(Cys)_4]$). Anaerobic addition of a solution of sodium dithionite rapidly bleached the visible electronic absorption spectrum of MBP-*Ec*FeoC (Fig. S3), caused the loss of this rubredoxin-like signal at $g \approx 4.3$, and gave rise to a weak rhombic EPR signal with g values of approximately 2.04, 1.93, and 1.89 (Fig. 5B). These values are similar to those observed for reduced $[4Fe\text{-}4S]^{+}$

clusters,[45-46] indicating that some $[4Fe\text{-}4S]^{2+}$ (EPR-silent until reduction to the +1 state) is present even after aerobic purification. Importantly, we observe no spectral evidence for the presence of a HiPIP cluster in our MBP-*Ec*FeoC construct under oxidizing or reducing conditions.[47] Taken together, it is clear that the aerobically-isolated MBP-*Ec*FeoC fusion purifies as an admixture of a rubredoxin-like cluster (likely deriving from decomposition of the higher-order [4Fe-4S] species) and a low amount of $[4Fe\text{-}4S]^{2+}$, indicating that a [4Fe-4S] cluster is plausibly present in this construct when expressed within the *E. coli* host prior to cell lysis.

Anaerobic reconstitution of cleaved EcFeoC yields a $[4Fe\text{-}4S]^{2+}$ cluster.

Because [Fe-S] clusters are generally oxygen sensitive,[48] because we observed sub-stoichiometric loading of our MBP-*Ec*FeoC fusion, and because our spectral characterization suggested the presence of a degraded cluster, we chose to anaerobically reconstitute our cleaved *Ec*FeoC construct, which very closely mimics the native *Ec*FeoC form. During the cleavage process, the TEV protease and fusion construct are both mixed in a buffer containing EDTA; however, after cleavage and separation, *Ec*FeoC still retains a small amount of iron that was not chelated during this process (0.04 ions ± 0.02 ions per polypeptide), which gives rise to the weak shoulder in the electronic absorption of the cleaved protein at $\lambda_{max} \approx 330$ nm (Fig, 3B). We then reconstituted the now-cleaved *Ec*FeoC by incubation with up to 6 mole equivalents of Fe^{3+} followed by 6 mole equivalents of S^{2-} with the cleaved protein. After centrifugation, filtration, and several rounds of buffer exchanges, the reconstituted protein bore a golden yellow color with a single $\lambda_{max} \approx 400$ nm in the visible region. The electronic absorption spectrum of reconstituted cleaved *Ec*FeoC (Fig. 3C) is distinct from the MBP-*Ec*FeoC (Fig. 3A), but bears a remarkable similarity to the $[4Fe\text{-}4S]^{2+}$-bound forms of FNR[49-50] and Endo III[51], strongly suggesting a

similar cluster composition bound to *Ec*FeoC. However, metal stoichiometry displayed prep-to-prep variation, with our best preps containing ≈ 3 Fe ions per polypeptide (2.6 ions ± 0.5 ions).

To confirm the presence of a $[4Fe\text{-}4S]^{2+}$ cluster and not a $[3Fe\text{-}4S]^{+}$ cluster, we then recorded and analyzed the XAS and EPR spectra of reconstituted *Ec*FeoC. The Fe edge EXAFS spectrum and best fits of anaerobically reconstituted *Ec*FeoC are shown in Fig. 4B and inset. Simulations of the EXAFS data again reveal only S-based environments as the nearest neighbor ligands with an average distance of 0.226 nm ± 0.005 nm (2.26 Å ± 0.05 Å) (Fig. 4B and inset, Table 1). The total Fe-S interactions are best fitted with a coordination number of 4, and long-range scattering interactions representing 1 Fe-Fe vector at 0.254 nm ± 0.005 nm (2.54 Å ± 0.05 Å) and 2 Fe-Fe vectors at 0.271 nm ± 0.005 nm (2.71 Å ± 0.05 Å) are now present (Fig. 4B and inset, Table 1), all consistent with the [4Fe-4S] designation and based on previous literature.[52] CW X-band EPR spectroscopy confirms this assignment and identifies the isolated form of anaerobically reconstituted *Ec*FeoC as a $[4Fe\text{-}4S]^{2+}$ cluster. The as-isolated form of reconstituted *Ec*FeoC has no EPR signal when analyzed over a range of 400 mT (Fig. 5C) at multiple temperature ranges, indicating that the cluster is in its oxidized state (*i.e.*, $[4Fe\text{-}4S]^{2+}$) and that no $[3Fe\text{-}4S]^{+}$ is present. Anaerobic addition of a solution of sodium dithionite bleached the visible electronic absorption spectrum of reconstituted *Ec*FeoC and gave rise to a narrow rhombic EPR signal with two distinct *g* values of approximately 2.04, 1.93, and a third *g* value at approximately 1.89 (Fig. 5D), very similar to other proteins that bind a $[4Fe\text{-}4S]^{+}$ clusters after chemical reduction.[45-46] Thus, these data clearly indicate that anaerobically reconstituted *Ec*FeoC binds a redox-active $[4Fe\text{-}4S]^{2+/+}$ cluster (not a HiPIP cluster) and, based on our Fe-to-polypeptide stoichiometry, suggest ≈ 75 % cluster incorporation.

The EcFeoC $[4Fe\text{-}4S]^{2+}$ cluster is oxygen-sensitive.

Given the striking similarity of the spectral properties of *Ec*FeoC and the cluster-binding transcriptional regulator FNR, we wondered whether reconstituted *Ec*FeoC would be oxygen-sensitive in a similar manner. This curiosity was further stimulated by the previous suggestion the *Kp*FeoC bore a HiPIP cluster with extremely unusual oxygen insensitivity ($t_{½}$ ≈ 14 h; *i.e.*, ≈ 804 min).[34] We initially removed samples of our anaerobically reconstituted *Ec*FeoC bearing $[4Fe\text{-}4S]^{2+}$ out of the glovebox and simply exposed the sample to ambient conditions while monitoring the electronic absorption features (Fig. S4A). Clearly divergent from *Kp*FeoC, upon exposure of *Ec*FeoC to air, we observed an isosbestic conversion of the electronic absorption features that indicated rapid (≈ 15 min for complete conversion) oxidative degradation of a $[4Fe\text{-}4S]^{2+}$ cluster (starting) to a distinctive $[2Fe\text{-}2S]^{2+}$ cluster (final),[50, 53-54] nicely mirroring the spectral behavior of FNR under similar conditions, albeit more slowly.[50, 54] The kinetics of this process are complex and include an initial lag phase (Fig. S4B), prompting us to wonder whether this slowly, multi-phasic process might be due to the limited oxygen diffusion into our previously anaerobic sample. To test this hypothesis, we repeated our cluster oxidation by mixing our anaerobic protein with air-saturated buffer. We noted a more rapid conversion from the $[4Fe\text{-}4S]^{2+}$ to the $[2Fe\text{-}2S]^{2+}$ cluster form (≈ 5 min for complete conversion, Fig. 6A and inset), which we fitted to a single exponential decay (Fig. 6B) with a k_{obs} of (0.037 ± 0.010) s^{-1} representing a $t_{½}$ of (19 ± 4.8) s. These results are in excellent agreement with those observed for the oxidation of FNR under O_2-saturated conditions, in which a k_{obs} ≈ 0.04 s^{-1} ($t_{½}$ ≈ 10.2 s) was reported.[54] Given the striking similarities between the two, we assume that the oxidative degradation of *Ec*FeoC follows a similar pattern as FNR in which the $[4Fe\text{-}4S]^{2+}$ cluster decomposition proceeds through a transient [3Fe-4S] cluster prior to formation of $[2Fe\text{-}2S]^{2+}$;[50] however, we have yet to detect a spectroscopic signal diagnostic of a [3Fe-4S] cluster, which

will require further investigation. Nevertheless, our data demonstrate that *Ec*FeoC $[4Fe\text{-}4S]^{2+}$ cluster is rapidly oxygen sensitive, strongly divergent from the previously reported behavior of *Kp*FeoC.[34]

The EcFeoC [4Fe-4S] cluster alters protein conformation but not oligomerization.

Despite unambiguous evidence that *Ec*FeoC binds a $[4Fe\text{-}4S]^{2+}$ cluster, metal analysis indicated a maximal Fe:polypeptide ratio of 2.6 ions ± 0.5 ions (i.e., 3 Fe ions per polypeptide) after anaerobic reconstitution. While it is not uncommon to produce apo protein during chemical reconstitution, this stoichiometry could indicate that binding of the [4Fe-4S] cluster initiates dimerization (*i.e.*, one [4Fe-4S] cluster per dimer), which we considered. Our initial studies of cleaved, aerobic apo *Ec*FeoC indicate that the protein migrates via gel filtration with a calculated molecular mass (≈ 9000 g/mol) (Fig. 2B) consistent with monomeric protein under aerobic conditions and in the presence (or absence) of reductant. However, due to experimental limitations and the rapid sensitivity to oxygen of our anaerobically reconstituted $[4Fe\text{-}4S]^{2+}$ form (*vide supra*), we could not repeat this experiment in the same manner. To circumvent this issue, we turned to dynamic light scattering (DLS), which we could adapt to anaerobic conditions in order to compare the size distribution of *Ec*FeoC in solution prior and after anaerobic reconstitution.

The results of our DLS studies support a change in protein conformation upon cluster binding, but our data are inconsistent with a model of cluster-mediated dimerization. DLS analysis of cleaved *Ec*FeoC by intensity (Fig. 7C) indicates high monodispersity with only minimal aggregation. When calculated by volume (Fig. 7B) or by number (Fig. 7A), the size distribution is dominated by scattering of a narrow ensemble of particles < 10 nm in diameter. Based on intensity, the distribution of cleaved apo *Ec*FeoC in solution is calculated to have an

ideal globular shape with a range of diameters ≈ 2.9 nm to 3.4 nm (29 Å to 34 Å). While it is known from NMR studies that the *Ec*FeoC protomer has an elongated rather than a globular shape (PDB ID 1XN7), this value is a useful benchmark to compare the behavior of the reconstituted protein. Even if a large amount of surface were buried, one would expect dimerization to increase the size of the DLS particle distribution modestly after anaerobic reconstitution if cluster-mediated oligomerization were operative. In fact, we observe exactly the opposite: upon reconstitution to the $[4Fe\text{-}4S]^{2+}$ *Ec*FeoC form, the uniformity remains comparable (Fig. 7C), while the calculated size distribution by volume (Fig. 7B) or by number (Fig. 7A) *decrease* modestly. Calculated based on volume or number, the globular diameter of the anaerobically-reconstituted *Ec*FeoC has contracted in size to ≈ 0.21 nm to 0.25 nm (21 Å to 25 Å). We attempted to do the same measurement after exposure of $[4Fe\text{-}4S]^{2+}$ *Ec*FeoC to oxygen to generate the $[2Fe\text{-}2S]^{2+}$ form; however, the analysis was hindered by the formation of an $FeS_{(s)}$ decomposition product of the oxidized $[4Fe\text{-}4S]^{2+}$ form and dominated the DLS measurements. Instead, we analyzed the more oxygen-stable $[2Fe\text{-}2S]^{2+}$ *Ec*FeoC form via SEC and noted a nearly identical retention volume (*i.e.,* size) to that of cleaved apo *Ec*FeoC prior to reconstitution (Fig. S5). Thus, our data indicate that *Ec*FeoC remains monomeric in all three oxidized forms studied here (apo, $[4Fe\text{-}4S]^{2+}$, and $[2Fe\text{-}2S]^{2+}$), but it appears that binding of the $[4Fe\text{-}4S]^{2+}$ cluster compacts the conformation of *Ec*FeoC compared to the apo form.

Discussion

In this work, we are the first to demonstrate that *Ec*FeoC binds an [Fe-S] cluster, and we have characterized the physical and electronic nature of this cluster extensively. When isolated aerobically, we show that the MBP-*Ec*FeoC fusion has spectral properties consistent with a mixture of redox-active $[4Fe\text{-}4S]^{2+/+}$ and rubredoxin-like clusters. We believe that the rubredoxin-like cluster derives from oxidative degradation of the [4Fe-4S] cluster during aerobic protein purification (Fig. 8). Anaerobic reconstitution of the cleaved *Ec*FeoC demonstrates binding of a redox-active $[4Fe\text{-}4S]^{2+/+}$ cluster, and we suggest this cluster composition is likely more operative within the prokaryotic cell under anaerobic and/or acidic conditions in which environmental Fe^{2+} is more prevalent and the *feo* operon is upregulated.[4, 7] This [4Fe-4S] cluster is also oxygen-sensitive, and our spectral data indicate a rapid (≈ 5 min for complete conversion) oxygen-mediated decomposition of the $[4Fe\text{-}4S]^{2+}$ cluster to a $[2Fe\text{-}2S]^{2+}$ cluster (Fig. 6). The observed *Ec*FeoC behavior is strongly reminiscent of the behavior of the transcriptional regulator FNR.[50, 54-55] However, divergent from FNR, we do not observe cluster-mediated dimerization;[50] rather, our DLS data suggest that *Ec*FeoC remains monomeric but changes conformation upon cluster binding in solution. Despite this finding, we cannot currently rule out the possibility that *Ec*FeoC may dimerize in the presence of DNA. Conversely, there are documented cases of transcriptional regulators that function as monomers,[56-57] and *Ec*FeoC could operate in this manner.

Our current work stands in strong contrast to the interpreted behavior of *Kp*FeoC, the only other spectroscopically characterized FeoC. In that previous work, the authors demonstrated that a tagged form of *Kp*FeoC purified with a sub-stoichiometric (less than approximately 10 %) admixture of multiple [Fe-S] cluster forms.[34] Based on EPR spectra and electronic absorption

data, it was concluded that the as-isolated *Kp*FeoC cluster was enriched in an unusual $[4Fe\text{-}4S]^{3+}$ HiPIP form that could also access the $[4Fe\text{-}4S]^{2+/+}$ redox states, and that this HiPIP cluster could have functional relevance.[34] This conclusion seems extremely unusual for a γ-proteobacterium such as *K. pneumoniae*, as HiPIP clusters are commonly found in photosynthetic and denitrifying bacteria because of their extremely positive reduction potentials (*ca*. +50 mV to +500 mV).[58-59] This highly-elevated redox potential is often used to drive electron transport within the respiratory and photosynthetic electron chains[59] and/or iron oxidation[60], precisely the opposite function of the Feo system, which maintains reduced iron stores. However, the electronic absorption and EPR data of *Kp*FeoC presented are inconsistent with any sort of [4Fe-4S] designation. The aerobically-isolated electronic absorption of *Kp*FeoC is distinct from spectra of pure $[4Fe\text{-}4S]^{2+}$ or $[2Fe\text{-}2S]^{2+}$ clusters, and instead suggests the presence of a mixture of species similar to our MBP-*Ec*FeoC construct.[34] Furthermore, aerobically-isolated *Kp*FeoC demonstrates an extremely weak, rhombic CW X-band EPR spectrum with g_1=2.060 and two overlapping values of g_2/g_3=2.007, with an increase in intensity with only a very modest shift upon dithionite reduction.[34] The shape of the spectrum and the narrow spread of the *g* values are more often observed in the common $[2Fe\text{-}2S]^{+}$ ferredoxin-like or $[4Fe\text{-}4S]^{+}$ cluster forms[45] rather than the much rarer $[4Fe\text{-}4S]^{3+}$ HiPIP form, which typically displays an axial spectrum of $g_1 \approx 2.12$ and $g_2/g_3 \approx 2.03$.[47] Only a narrow EPR window (≈ 280 mT to 400 mT) was reported for *Kp*FeoC, so it is unclear whether any additional features at $g \approx 4.3$ were present. Further calling into question this assignment is the unusual oxygen-stability of the *Kp*FeoC cluster under atmospheric conditions at 4 °C in which a $t_{½}$ of ≈ 14 h to 18 h (*e.g.*, 840 min to 1080 min) was reported.[34] Although there are reports of oxygen-tolerant [Fe-S] clusters,[61] given the low percentage of cluster loading along with spectral features that are inconsistent with a [4Fe-4S] cluster, it is

possible that these data were used to incorrectly assign a HiPIP [4Fe-4S]$^{3+}$ cluster. Further work on *Kp*FeoC will be necessary to discern whether this behavior is reproducible under strict anaerobic conditions or instead resembles our observations on *Ec*FeoC.

Based on our current data and in conjunction with previous observations, we posit a working hypothesis in which the cluster-binding FeoCs may function as *in vivo* iron sensors. In *E. coli*, the *feo* operon is under control of both FUR and FNR regulation[9, 22]: under low iron conditions, *feo* regulation is derepressed by dissociation of FUR; upon switching from aerobic to anaerobic metabolism, *feo* is upregulated in response to FNR binding.[7, 22] As FeoB-mediated ferrous iron import increases the labile ferrous iron pool within the cytosol, FeoC could receive iron directly from FeoB and become replete with its [4Fe-4S] cluster. Based on our data, this binding is associated with conformational changes of the FeoC polypeptide, most likely within the "wing" of the winged-helix motif, which is otherwise disordered (*i.e.*, extremely dynamic) in the apo form based on its NMR structure (Fig. 1C).

Following this binding event, there are several possible cellular responses that FeoC could elicit. In one scenario, this conformational change could either target FeoC to, or could release FeoC binding from, the cytosolic side of the membrane transporter FeoB. This process could alter FeoB-mediated ferrous iron import, or even allow for the targeting of FeoB for proteolytic degradation, as has been suggested based on studies in *S. enterica*.[62] Another possibility includes that cluster binding functions as an "on" switch for transcriptional repression of the *feo* operon. We favor this theory based on the winged-helix fold of FeoC, common to many transcriptional regulators, and the N-terminal location of the helix-turn-helix domain of this fold (Fig. 1C), which suggests a repressor function by comparison to analogous regulators.[63] At high levels of labile intracellular ferrous iron, [4Fe-4S]-replete FeoC could target the *feo*

operon specifically for repression in lieu of upstream dissociation of the global regulator FNR, which is driving transcription of multiple anaerobic processes across the cellular landscape.[55] In this scenario, once *E. coli* were to switch back to aerobic metabolism, both FeoC and FNR would be rapidly deactivated as their clusters would be oxidized and degraded (Fig. 8), and our data demonstrate that the oxidation of the clusters in these two proteins are nicely matched at the kinetic regime. In FNR, cluster oxidation is accompanied by loss of dimerization and transcriptional deactivation.[64] FeoC could function similarly in the presence of DNA, or a conformational change upon cluster oxidation could drive dissociation from DNA. Thus, FeoC would provide an opportunity for *E. coli* to dynamically fine-tune its level of ferrous iron import under anaerobic conditions independent of FNR functionality. On the one hand, mutation of the *Y. pestis feoC* gene supports this theory, as this mutant displayed overexpression of *feoA* and *feoB* genes,[65] and there is a promoter region that overlaps with *fnr* for which no regulator has been identified.[66] Additionally, FeoC deletion leads to high intracellular levels of ferrous iron in *S. enterica*,[62] suggesting a regulatory mechanism has been removed to control ferrous iron uptake. On the other hand, there are some FeoCs (*e.g.*, *V. cholerae*) that have no Cys residues, precluding cluster binding. It is possible that *Vc*FeoC could function as a transcriptional regulator by dimerizing on its own, rather than in a cluster-mediated manner. However, cellular studies of *Vc*FeoC have indicated that this protein binds directly to FeoB and may have a divergent function from those FeoCs that bind [Fe-S] clusters,[25, 67] which could be multifunctional. Testing these intriguing hypotheses relating to FeoC represent exciting future avenues in the study of the Feo system.

Acknowledgements

This work was supported by NSF CAREER grant 1844624 (A. T. S.), and in part by NIH-NIGMS grant T32 GM066706 (A. E. S.). Sequence searches utilized both database and analysis functions of the Universal Protein Resource (UniProt) Knowledgebase and Reference Clusters (http://www.uniprot.org) and the National Center for Biotechnology Information (http://www.ncbi.nlm.nih.gov/). Use of the Stanford Synchrotron Radiation Lightsource, SLAC National Accelerator Laboratory, is supported by the U.S. Department of Energy, Office of Science, Office of Basic Energy Sciences under Contract No. DE-AC02-76SF00515. The SSRL Structural Molecular Biology Program is supported by the DOE Office of Biological and Environmental Research, and by the National Institutes of Health, National Institute of General Medical Sciences (including P41 GM103393).

The authors declare no competing financial interests.

Supporting Information

Supporting information is available free of charge online:

SDS-PAGE and SEC analyses of MBP-*Ec*FeoC prior to and post cleavage (Fig. S1)

Far-UV CD spectra of cleaved, apo *Ec*FeoC (Fig. S2)

Electronic absorption spectra of as-isolated MBP-*Ec*FeoC prior and post reaction with sodium dithionite (Fig. S3)

Spectral and kinetics data of oxygen-sensitive $[4Fe\text{-}4S]^{2+}$ *Ec*FeoC after exposure to ambient conditions (Fig. S4)

SEC analyses of *Ec*FeoC after cluster conversion of $[4Fe\text{-}4S]^{2+}$ to $[2Fe\text{-}42]^{2+}$ (Fig. S5)

References

1. Andrews, S. C.; Robinson, A. K.; Rodríguez-Quiñones, F., Bacterial iron homeostasis. *FEMS Microbiol. Rev.* **2003,** *27*, 215-237.
2. Ganz, T., Iron homeostasis: fitting the puzzle pieces together. *Cell Metab.* **2008,** *7*, 288-290.
3. Coffey, R.; Ganz, T., Iron homeostasis: an anthropocentric perspective. *J. Biol. Chem.* **2017,** *292* (31), 12727-12734.
4. Velayudhan, J.; Hughes, N. J.; McColm, A. A.; Bagshaw, J.; Clayton, C. L.; Andrews, S. C.; Kelly, D. J., Iron acquisition and virulence in *Helicobacter pylori*: a major role for FeoB, a high-affinity ferrous iron transporter. *Mol. Microbiol.* **2000,** *37* (2), 274-286.
5. Wilks, A.; Burkhard, K. A., Heme and virulence: how bacterial pathogens regulate, transport and utilize heme. *Nat. Prod. Rep.* **2007,** *24*, 511-522.
6. Reinhart, A. A.; Oglesby-Sherrouse, A. G., Regulation of *Pseudomonas aeruginosa* virulence by distinct iron sources. *Genes* **2016,** *7* (12), E126.
7. Sestok, A. E.; Linkous, R. O.; Smith, A. T., Toward a mechanistic understanding of Feo-mediated ferrous iron uptake. *Metallomics* **2018,** *10*, 887-898.
8. Cartron, M. L.; Maddocks, S.; Gillingham, P.; Craven, C. J.; Andrews, S. C., Feo-Transport of ferrous iron into bacteria. *Biometals* **2006,** *19*, 143-157.
9. Hantke, K., Ferrous iron transport mutant in *Escherichia coli* K12. *FEMS Microbiol. Lett.* **1987,** *44*, 53-57.
10. Smith, A. T.; Sestok, A. E., Expression and Purification of Functionally Active Ferrous Iron Transporter FeoB from *Klebsiella pneumoniae*. *Protein Expr. Purif.* **2018,** *142*, 1-7.

11. Sassone-Corsi, M.; Chairatana, P.; Zheng, T.; Perez-Lopez, A.; Edwards, R. A.; George, M. D.; Nolan, E. M.; Raffatellu, M., Siderophore-based immunization strategy to inhibit growth of enteric pathogens. *Proc. Natl. Acad. Sci. U.S.A.* **2016,** *113* (47), 13462-13467.

12. Miethke, M.; Marahiel, M. A., Siderophore-Based Iron Acquisition and Pathogen Control. *Microbiol. Mol. Biol. Rev.* **2007,** *71* (3), 413-451.

13. Wandersman, C.; Delepelaire, P., Bacterial Iron Sources: From Siderophores to Hemophores. *Annu. Rev. Microbiol.* **2004,** *58*, 611-647.

14. Kim, H.; Lee, H.; Shin, D., The FeoA protein is necessary for the FeoB transporter to import ferrous iron. *Biochem. Biophys. Res. Com.* **2012,** *423*, 733-738.

15. Dashper, S. G.; Ang, C. S.; Veith, P. D.; Mitchell, H. L.; Lo, A. W.; Seers, C. A.; Walsh, K. A.; Slakeski, N.; Chen, D.; Lissel, J. P.; Butler, C. A.; O'Brien-Simpson, N. M.; Barr, I. G.; Reynolds, E. C., Response of *Porphyromonas gingivalis* to heme limitation in continuous culture. *J. Bacteriol.* **2009,** *191* (3), 1044-1055.

16. Dashper, S. G.; Butler, C. A.; Lissel, J. P.; Paolini, R. A.; Hoffmann, B.; Veith, P. D.; O'Brien-Simpson, N. M.; Snelgrove, S. L.; Tsiros, J. T.; Reynolds, E. C., A novel *Porphyromonas gingivalis* FeoB plays a role in manganese accumulation. *J. Biol. Chem.* **2005,** *280* (30), 28095-28102.

17. Pérez, N.; Johnson, R.; Sen, B.; Ramakrishnan, G., Two parallel pathways for ferric and ferrous iron acquisition support growth and virulence of the intracellular pathogen *Francisella tularensis* Schu S4. *MicrobiologyOpen* **2016,** *5* (3), 453-468.

18. Sankari, S.; O'Brian, M. R., The *Bradyrhizobium japonicum* ferrous iron transporter FeoAB is required for ferric iron utilization in free living aerobic cells and for symbosis. *J. Biol. Chem.* **2016,** *291* (30), 15653-15662.

19. Stojiljkovic, I.; Cobeljic, M.; Hantke, K., *Escherichia coli* K-12 ferrous iron uptake mutants are impaired in their ability to colonize the mouse intestine. *FEMS Microbiol. Lett.* **1993,** *108* (1), 111-115.

20. Tsolis, R. M.; Baumler, A. J.; Heffron, F.; Stojiljkovic, I., Contribution of TonB- and Feo-mediated iron uptake to growth of *Salmonella typhimurium* in the mouse. *Infect. Immun.* **1996,** *64*, 4549-4556.

21. Naikare, H.; Palyada, K.; Panciera, R.; Marlow, D.; Stintzi, A., Major Role for FeoB in *Campylobacter jejuni* Ferrous Iron Acquisition, Gut Colonization, and Intracellular Survival. *Infect. Immun.* **2006,** *74* (10), 5433-5444.

22. Kammler, M.; Schön, C.; Hantke, K., Characterization of the ferrous iron uptake system of *Escherichia coli*. *J. Bacteriol.* **1993,** *175* (19), 6212-6219.

23. Thomas-Charles, C. A.; Zheng, H.; Palmer, L. E.; Mena, P.; Thanassi, D. G.; Furie, M. B., FeoB-mediated uptake of iron by *Francisella tularensis*. *Infect. Immun.* **2013,** *81* (8), 2828-2837.

24. Runyen-Janecky, L. J.; Reeves, S. A.; Gonzales, E. G.; Payne, S. M., Contribution of the *Shigella flexneri* Sit, Iuc, and Feo iron acquisition systems to iron acquisition in vitro and in cultured cells. *Infect. Immun.* **2003,** *71* (4), 1919-1928.

25. Weaver, E. A.; Wyckoff, E. E.; Mey, A. R.; Morrison, R.; Payne, S. M., FeoA and FeoC are essential components of the *Vibrio cholerae* ferrous iron uptake system, and FeoC interacts with FeoB. *J. Bacteriol.* **2013,** *195* (21), 4826-4835.

26. Perry, R. D.; Mier Jr., I.; Fetherston, J. D., Roles of the Yfe and Feo transporters of *Yersinia pestis* in iron uptake and intracellular growth. *Biometals* **2007,** *20*, 699-703.

27. Cornelis, P.; Dingemans, J., *Pseudomonas aeruginosa* adapts its iron uptake strategies in function of the type of infections. *Front. Cell. Infect. Microbiol.* **2013,** *3*, 1-7.

28. Minandri, F.; Imperi, F.; Frangipani, E.; Bonchi, C.; Visaggio, D.; Facchini, M.; Pasquali, P.; Brangozi, A.; Visca, P., Role of the iron uptake systems in *Pseudomonas aeruginosa* virulence and airway infection. *Infect. Immun.* **2016,** *84*, 2324-2335.

29. Hunter, R. C.; Asfour, F.; Dingemans, J.; Osuna, B. L.; Samad, T.; Malfroot, A.; Cornelis, P.; Newman, D. K., Ferrous iron is a significant component of bioavailable iron in cystic fibrosis airways. *mBio* **2013,** *4* (4), e00557-13.

30. Banin, E.; Vasil, M. L.; Greenberg, E. P., Iron and *Pseudomonas aeruginosa* biofilm formation. *Proc. Natl. Acad. Sci. U.S.A.* **2005,** *102* (31), 11076-11087.

31. Singh, P. K.; Parsek, M. R.; Greenberg, E. P.; Welsh, M. J., A component of innate immunity prevents bacterial biofilm development. *Nature* **2002,** *417*, 552-555.

32. Lau, C. K. Y.; Krewulak, K. D.; Vogel, H. J., Bacterial ferrous iron transport: the Feo system. *FEMS Microbiol. Rev.* **2016,** *40*, 273-298.

33. Hung, K.-W.; Juan, T.-H.; Hsu, Y.-L.; Huang, T. H., NMR structure note: the ferrous iron transport protein C (FeoC) from *Klebsiella pneumoniae J. Biolmol. NMR* **2012,** *53*, 161-165.

34. Hsueh, K.-L.; Yu, L.-K.; Chen, Y.-H.; Cheng, Y.-H.; Hsieh, Y.-C.; Ke, S.-c.; Hung, K.-W.; Chen, C.-J.; Huang, T.-H., FeoC from *Klebsiella pneumoniae* Contains a [4Fe-4S] Cluster. *J. Bacteriol.* **2013,** *195* (20), 4726-4734.

35. Riemer, J.; Hoepken, H. H.; Czerwinska, H.; Robinson, S. R.; Dringen, R., Colorimetric ferrozine-based assay for the quantitation of iron in cultured cells. *Anal. Biochem.* **2004,** *331* (2), 370-375.

36. Jeitner, T. M., Optimized ferrozine-based assay for dissolved iron. *Anal. Biochem.* **2014,** *454* (1), 36-37.

37. George, G. N. *EXAFSPAK*, Stanford Synchrotron Radiation Laboratory: Menlo Park, CA, 1995.

38. Binsted, N.; Hasnain, S. S., State-of-the-art analysis of whole X-ray absorption spectra. *J. Synchrotron. Radiat.* **1996,** *3*, 185-196.

39. Gurman, S. J.; Binsted, N.; Ross, I., A rapid, exact curved-wave theory for EXAFS calculations. *J. Phys. C.* **1984,** *17*, 143-151.

40. Gurman, S. J.; Binsted, N.; Ross, I., A rapid, exact, curved-wave theory for EXAFS calculations. II. The multiple-scattering contributions. *J. Phys. C.* **1986,** *19*, 1845-1861.

41. Crack, J. C.; Green, J.; Thomson, A. J.; Le Brun, N. E., Iron-sulfur clusters as biological sensors: the chemistry of reastions with moleculer oxygen and nitric oxide. *Acc. Chem. Res.* **2014,** *47*, 3196-3205.

42. Johnson, D. C.; Dean, D. R.; Smith, A. D.; Johnson, M. K., Structure, function, and formation of biological iron-sulfur clusters. *Annu. Rev. Biochem.* **2005,** *74*, 247-281.

43. Ugulava, N. B.; Gibney, B. R.; Jarrett, J. T., Biotin synthase contains two distinct iron-sulfur cluster binding site: chemical and spetroelecrochemical analysis of iron-sulfur cluster interconversions. *Biochemistry* **2001,** *40*, 8343-8351.

44. Peisach, J.; Blumberg, B.; Lode, E. T.; Coon, M. J., An analysis of the electron paramagneitc resonance spectrum of *Pseudomonas oleovorans* rubredoxin. A method for determinsation of the the ligands of ferric iron in completely rhombic sites. *J. Biol. Chem.* **1971,** *246* (19), 5877-5881.

45. Guigliarelli, B.; Bertrand, P., Application of EPR spectroscopy to the structural and functional study of iron-sulfur proteins. *Adv. Inorg. Chem.* **1999,** *47*, 421-497.

46. Cammack, R., Iron-sulfur clusters in enzymes: themes and variations. *Adv. Inorg. Chem.* **1992,** *38*, 281-322.

47. Priem, A. H.; Klaassen, A. A. K.; Reijerse, E. J.; Meyer, T. E.; Luchinat, C.; Capozzi, F.; Dunham, W. R.; Hagen, W. R., EPR analysis of multiple forms of $[4Fe\text{-}4S]^{3+}$ clusters in HiPIPs. *J. Biol. Inorg. Chem.* **2005,** *10*, 417-424.

48. Imlay, J. A., Iron-sulphur clusters and the problem with oxygen. *Mol. Microbiol.* **2006,** *59* (4), 1073-1082.

49. Green, J.; Bennet, B.; Jordan, P.; Ralph, E. T.; Thomson, A. J.; Guest, J. R., Reconstitution of the [4Fe-4S] cluster in FNR and demonstration of the aerobic-anaerobic transcription switch *in vitro*. *Biochem. J.* **1996,** *316*, 887-892.

50. Crack, J. C.; Stapleton, M. R.; Green, J.; Thomson, A. J.; Le Brun, N. E., Influence of association state and DNA binding on the O_2-reactivity of [4Fe-4S] fumarate and nitrate reduction (FNR) regulation. *Biochem. J.* **2014,** *463*, 83-92.

51. Tse, E. C. M.; Zwang, T. J.; Barton, J. K., The oxidation state of [4Fe4S] clusters modulates the DNA-binding affinity of DNA repair proteins. *J. Am. Chem. Soc.* **2017,** *139* (36), 12784-12792.

52. Silver, S. C.; Gardenghi, D. J.; Naik, S. G.; Shepard, E. M.; Huynh, B. H.; Szilagyi, R. K.; Broderick, J. B., Combined Mössbauer spectroscopic, multi-edge X-ray absorption spectroscopic, and density functional theoretical study of the radical SAM enzyme spore photoproduct lyase. *J. Biol. Inorg. Chem.* **2014,** *19*, 465-483.

53. Rajakovich, L. J.; Nørgaard, H.; Warui, D. M.; Chang, W.-c.; Li, N.; Booker, S. J.; Krebs, C.; Bollinger, J., J. Martin; Pandelia, M.-E., Rapid reduction of the diferric-peroxyhemiacetal intermediate in aldehyde-deformylating oxygenase by a cyanobacterial ferredoxin: evidence for a free-radical mechanism. *J. Am. Chem. Soc.* **2015,** *137*, 11695-11709.

54. Sutton, V. R.; Mettert, E. L.; Beinert, H.; Kiley, P. J., Kinetic analysis of the oxidative conversion of the $[4Fe\text{-}4S]^{2+}$ cluster of FNR to a $[2Fe\text{-}2S]^{2+}$ cluster. *J. Bacteriol.* **2004,** *186* (23), 8018-8025.

55. Crack, J.; Green, J.; Thomson, A. J., Mechanism of Oxygen Sensing by the Bacterial Transcription Factor Fumarate-Nitrate Reduction (FNR). *J. Biol. Chem.* **2004,** *279* (10), 9278-9286.

56. Feng, L.; Chen, Z.; Hu, Y.; Chen, S., Genome-wide characterization of monomeric transcriptional regulators in *Mycobacterium tuberculosis*. *Microbiology* **2016,** *162* (5), 889-897.

57. Richet, E.; Raibaud, O., Purification and properties of the MalT protein, the transcription activator of the *Escherichia coli* maltose regulon. *J. Biol. Chem.* **1987,** *262* (26), 12647-12653.

58. Tedro, S. M.; Meyer, T. E.; Bartsch, R. G.; Kamen, M. D., Primary structures of high potential, four-iron-sulfur ferredoxins from the purple sulfur photosynthetic bacteria, *Thiocapso roseopersicina* and *Chromatium gracile*. *J. Biol. Chem.* **1981,** *256* (2), 731-735.

59. Bonora, P.; Principi, I.; Monti, B.; Ciurli, S.; Zannoni, D.; Hochkoeppler, A., On the role of high-potential iron-sulfur proteins and cytochromes in the respiratory chain of two facultative phototrophs. *Biochim. Biophys. Acta, Bioenergetics* **1999,** *1410* (1), 51-60.

60. Ilbert, M.; Bonnefoy, V., Insight into the evolution of the iron oxidation pathways. *Biochim. Biophys. Acta, Bioenergetics* **2013,** *1827* (2), 161-175.

61. Pandelia, M.-E.; Nitschke, W.; Infossi, P.; Giudici-Orticoni, M.-T.; Bill, E.; Lubitz, W., Characterization of a unique [FeS] cluster in the electron transfer chain of the oxygen tolerant [NiFe] hydrogenase from *Aquifex aeolicus*. *Proc. Natl. Acad. Sci. U.S.A.* **2011,** *108* (15), 6097-6102.

62. Kim, H.; Lee, H.; Shin, D., The FeoC Protein Leads to High Cellular Levels of the Fe(II) Transporter FeoB by Preventing FtsH Protease Regulation of FeoB in *Salmonella enterica*. *J. Bacteriol.* **2013,** *195* (15), 3364-3370.

63. Aravind, L.; Anantharaman, V.; Balaji, S.; Babu, M. M.; Iyer, L. M., The many faces of the helix-turn-helix doman: transcriptional regulation and beyond. *FEMS Microbiol. Rev.* **2005,** *29* (2), 231-262.

64. Khoroshilova, N.; Beinert, H.; Kiley, P. J., Association of polynuclear iron-sulfur center with a mutant FNR protein enhances DNA-binding. *Proc. Natl. Acad. Sci. U.S.A.* **1995,** *92*, 2499-2503.

65. Guo, J.; Nair, M. K. M.; Galván, E. M.; Liu, S.-L.; Schifferli, D. M., Tn5AraOut mutagenesis for the identification of *Yersinia pestis* genes involved in resistance towards cationic antimicrobial peptides. *Microb. Path.* **2011,** *51* (3), 121-132.

66. O'Connor, L.; Fetherston, J. D.; Perry, R. D., The *feoABC* locus of *Yersinia pestis* likely has two promoters causing unique iron regulation. *Front. Cell. Infect. Microbiol.* **2017,** *7* (331), eCollection 2017.

67. Stevenson, B.; Wyckoff, E. E.; Payne, S. M., *Vibrio cholerae* FeoA, FeoB, and FeoC interact to form a complex. *J. Bacteriol.* **2016,** *198* (7), 1160-1170.

Table 1. Fits obtained for the Fe K-EXAFS of the as-isolated MBP-*Ec*FeoC and cleaved anaerobically reconstituted *Ec*FeoC by curve fitting using the program EXCURVE 9.2.

		Fe-S			Fe-Fe			Fe-Fe			E_o[e]
Sample/fit	**Fit index[a]**	**No[b]**	**R[c] (nm) [Å]**	**DW[d] (nm^2) [$Å^2$]**	**No**	**R (nm) [Å]**	**DW (nm^2) [$Å^2$]**	**No**	**R (nm) [Å]**	**DW (nm^2) [$Å^2$]**	
MBP-*Ec*FeoC	0.75	3	0.226 [2.26]	0.00011 [0.011]	1	0.272 [2.72]	0.00005 [0.005]				0.7426
Cleaved reconstituted *Ec*FeoC	0.49	4	0.226 [2.26]	0.00011 [0.012]	2	0.271 [2.71]	0.00005 [0.005]	1	0.2451 [2.541]	0.00004 [0.004]	2.2563

[a]The least-squares fitting parameter (see *Materials and Methods*) [b]Coordination number [c]Bond length [d]Debye-Waller factor [e]Photoelectron energy threshold

Figure Legends

Figure 1. The Feo system and the structure of *E. coli* FeoC. **A**. The arrangement of the *feo* operon in *E. coli*, which encodes for three proteins: FeoA, FeoB, FeoC. **B**. Cartoon of the Feo system in *E. coli*. FeoA (red) and FeoC (green) are small cytosolic proteins that may function as regulatory accessories to control ferrous (Fe^{2+}) iron transport. Movement of ferrous iron across a cellular membrane is accomplished by the large, polytopic membrane protein FeoB (purple). Hydrolysis of GTP to GDP within the N-terminal soluble GTP-binding domain of FeoB (NFeoB, teal) is thought to regulate opening and closing of FeoB, but it is unknown whether this process is driven in an active or facilitated manner. **C**. Lowest-energy NMR conformer of *Ec*FeoC (PDB ID 1XN7). Labeled regions are: the helix-turn-helix (HTH) motif and the unstructured wing region that contains four Cys residues (Cys^{56}, Cys^{61}, Cys^{64} and Cys^{70}) involved in [Fe-S] cluster binding. The labels "N" and "C" represent the amino and carboxy termini, respectively.

Figure 2. Construct design and purification of *Ec*FeoC. **A**. Because of poor native expression, *Ec*FeoC was expressed as a maltose-binding protein (MBP; salmon) fusion (MBP-*Ec*FeoC). On the N-terminus is encoded an additional $(His)_6$ tag (purple) for orthogonal purification. Preceding the *Ec*FeoC portion of the polypeptide (green) is an encoded TEV protease cleavage site. **B**. Cleaved, purified *Ec*FeoC is monomeric (≈ 9000 g/mol, 9 kDa) based on its gel-filtration retention volume on Superdex 75. The compared standards (K_{av} versus log MW, linearity R^2=0.97) are: blue dextran (void), alcohol dehydrogenase (150000 g/mol, 150 kDa), bovine serum albumin (66000 g/mol, 66 kDa), carbonic anhydrase (29000 g/mol, 29 kDa), cytochrome *c* (12000 g/mol, 12 kDa), and aprotinin (6500 g/mol, 6.5 kDa). **C**. SDS-PAGE analysis (acrylamide mass fraction of 15 %, left panel) and Tris-tricine gel analysis (gradient of

acrylamide mass fraction from 10 % to 20 %, right panel), demonstrating *Ec*FeoC purity after cleavage and SEC. Black arrows indicate the location of the purified *Ec*FeoC. A small amount of dimeric *Ec*FeoC (≈ 18000 g/mol, 18 kDa) is observed in the Tris-tricine analysis at high protein concentration, but this dimeric species is only observed after freeze-thawing of the protein and cannot be dissociated by sample boiling.

Figure 3. Electronic absorption spectroscopy of *Ec*FeoC species suggests the presence of [Fe-S] clusters. **A**. Absorption spectrum of the MBP-*Ec*FeoC fusion protein aerobically as-isolated. **B**. Absorption spectrum of the cleaved apo *Ec*FeoC protein. **C**. Absorption spectrum of the cleaved, anaerobically reconstituted *Ec*FeoC protein. Solutions were kept at room temperature in a UV-transparent cuvette, and protein concentrations were generally 1 μmol/L to 20 μmol/L. Sample **A** was in MBP elution buffer, sample **B** was in TEV cleavage buffer, and sample **C** was in anaerobic reconstitution buffer (see Materials and Methods). Absorption data are normalized to the most intense band corresponding to the protein absorbance (280 nm).

Figure 4. X-ray absorption spectroscopy (XAS) indicates the presence of [Fe-S] clusters in *Ec*FeoC. Fe K-edge X-ray absorption fine structure (EXAFS) and Fourier transforms of MBP-*Ec*FeoC (**A**) and anaerobically reconstituted *Ec*FeoC (**B**). For ease of interpretation, data are graphed as Fourier transform amplitude versus distance (R) in Å, where 1 Å = 0.1 nm. Black traces represent the experimental data, and red traces represent the simulations. Parameters used to generate the simulated spectra are listed in Table 1. Sample **A** was in 25 mmol/L Tris buffer, pH 7.5, 200 mmol/L NaCl, 10 mmol/L maltose, 3.6 mol/L ethylene glycol (20% (v/v)), and 0.7

mol/L glycerol (5% (v/v)). Sample **B** was in 50 mmol/L MOPS buffer, pH 7.5, 150 mmol/L NaCl, 10 mmol/L DTT, and 3.6 mol/L ethylene glycol (20% (v/v)).

Figure 5. Electron paramagnetic resonance (EPR) spectroscopy indicates the identity of the observed [Fe-S] clusters in *Ec*FeoC. Continuous-wave (CW) X-band EPR spectra of MBP-*Ec*FeoC as-isolated (**A**), MBP-*Ec*FeoC reduced with sodium dithionite (**B**), cleaved and anaerobically-reconstituted *Ec*FeoC (**C**), and cleaved and anaerobically-reconstituted *Ec*FeoC reduced with sodium dithionite (**D**). Samples **A** and **B** were in 25 mmol/L Tris buffer, pH 7.5, 200 mmol/L NaCl, 10 mmol/L maltose, 3.6 mol/L ethylene glycol (20% (v/v) ethylene glycol), and 0.7 mol/L glycerol (5% (v/v) glycerol) ± 1 mmol/L sodium dithionite, respectively. Samples **C** and **D** were in 50 mmol/L MOPS buffer, pH 7.5, 150 mmol/L NaCl, 10 mmol/L DTT, and 3.6 mol/L ethylene glycol (20% (v/v) ethylene glycol) ± 1 mmol/L sodium dithionite, respectively. Samples **A** and **C** are plotted on identical scales, and samples **B** and **D** are plotted on identical scales. Spectral parameters were as follows: (**A**) 20 K, modulation amplitude = 0.5 mT, modulation frequency = 100 kHz, 1024 points, conversion time = 117.19 ms, microwave power = 9.5 mW, 4 scans (**B**) 20 K, modulation amplitude = 0.5 mT, modulation frequency = 100 kHz, 1024 points, conversion time = 87.89 ms, microwave power = 9.5 mW, 16 scans (**C**) 6 K, modulation amplitude = 0.5 mT, modulation frequency = 100 kHz, 1024 points; conversion time = 117.19 ms, microwave power = 4.7 mW, 1 scan (**D**) 6 K, modulation amplitude 0.5 mT, modulation frequency = 100 kHz, 1024 points, conversion time = 87.89 ms, microwave power = 1.9 mW, 16 scans. A cavity contaminant at ≈ 335 mT (g ≈ 2.005) was observed even after background subtraction in all spectra.

Figure 6. The $[4Fe\text{-}4S]^{2+}$ cluster of *Ec*FeoC is rapidly oxygen sensitive. **A**. Representative time course spectra of cleaved, anaerobically reconstituted *Ec*FeoC reacting with air-saturated buffer. Spectra were taken every 6 s (black, dotted) immediately after buffer mixing until reactivity stopped (≈ 5 min). The $[4Fe\text{-}4S]^{2+}$ spectral features (goldenrod) are rapidly lost and the appearance of the $[2Fe\text{-}2S]^{2+}$ spectral features rapidly appear (purple). The inset represents the plots of the two species before (goldenrod) and after (purple) reaction. The sample was in 50 mmol/L MOPS buffer, pH 7.5, 150 mmol/L NaCl, and 1 mmol/L DTT at room temperature. **B**. Representative plot of the kinetic decay of the absorbance feature at 400 nm (closed circles), characteristic of the $[4Fe\text{-}4S]^{2+}$ cluster, and its fitted simulation (black dashed line), revealing a k_{obs} of (0.037 ± 0.010) s^{-1} and a $t_{½}$ of (19 ± 4.8) s when averaged over three replicates.

Figure 7. *Ec*FeoC does not dimerize in the presence of the $[4Fe\text{-}4S]^{2+}$ cluster. Representative dynamic light scattering (DLS) data of apo (dashed) and $[4Fe\text{-}4S]^{2+}$-bound forms (solid) of *Ec*FeoC plotted as number (**A**), volume (**B**), or intensity (**C**) versus globular diameter, clearly demonstrating the cluster-bound form assumes a more compact shape than the apo form of *Ec*FeoC. Samples were in 50 mmol/L MOPS buffer, pH 7.5, 150 mmol/L NaCl, and 1 mmol/L DTT at room temperature.

Figure 8. The observed forms of the redox-active, oxygen-sensitive cluster in *Ec*FeoC. Under strictly anaerobic conditions (such as those that may be operative within *E. coli* during anaerobic growth), a $[4Fe\text{-}4S]^{2+/+}$ cluster is observed. Upon reaction with oxygen-replete buffer, the $[4Fe\text{-}4S]^{2+}$ rapidly decays to a $[2Fe\text{-}2S]^{2+}$ cluster. After prolonged exposure to oxygen, a rubredoxin-like decay product (*i.e.*, $[Fe^{3+}(Cys)_4]$) is observed. Unlike FNR, we have yet to observe a [3Fe-

4S]$^{+/0}$ cluster bound to *Ec*FeoC (indicated by the presence of brackets), but we surmise the transformation from [4Fe-4S]$^{2+}$ to [2Fe-2S]$^{2+}$ contains this transient species. This oxygen-responsive cluster disassembly may represent the behavior *Ec*FeoC undergoes *in vivo* during the organism's transition from anaerobic growth to aerobic growth.

Figure 1.

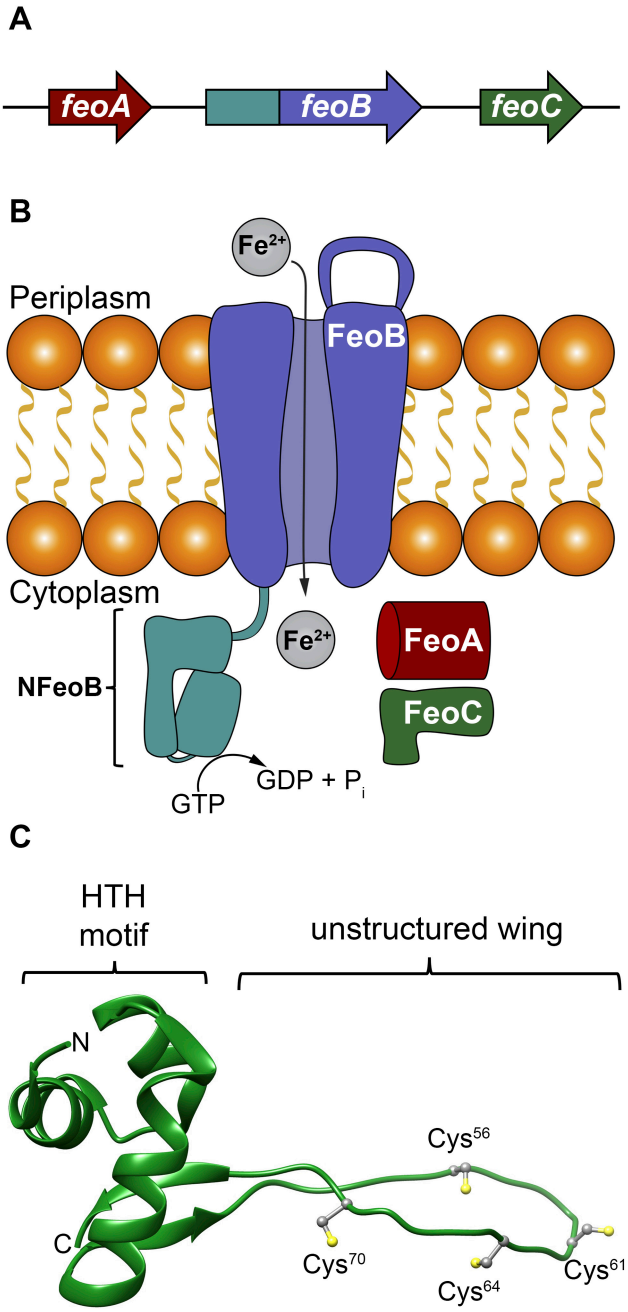
A
feoA
feoB
feoC
B
Fe2+
Periplasm
FeoB
Cytoplasm
Fe2+
FeoA
NFeoB
FeoC
GTP
GDP + Pi
C
HTH
motif
unstructured wing
N
C
Cys56
Cys70
Cys64
Cys61

Figure 2.

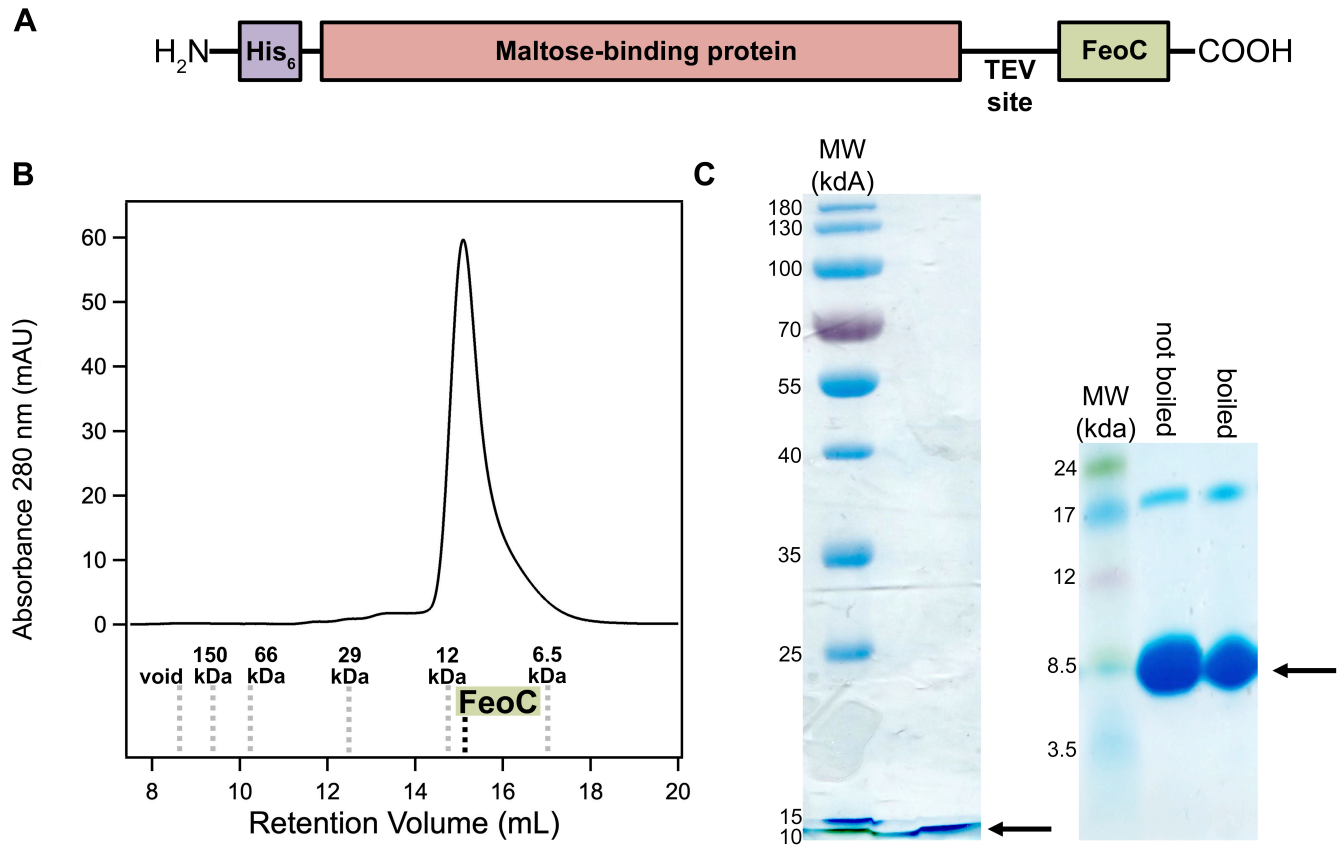
A
H2N
His6
Maltose-binding protein
TEV site
FeoC
COOH
B
Absorbance 280 nm (mAU)
Retention Volume (mL)
void
150 kDa
66 kDa
29 kDa
12 kDa
6.5 kDa
FeoC
C
MW (kdA)
180
130
100
70
55
40
35
25
15
10
MW (kda)
not boiled
boiled
24
17
12
8.5
3.5

Figure 3.

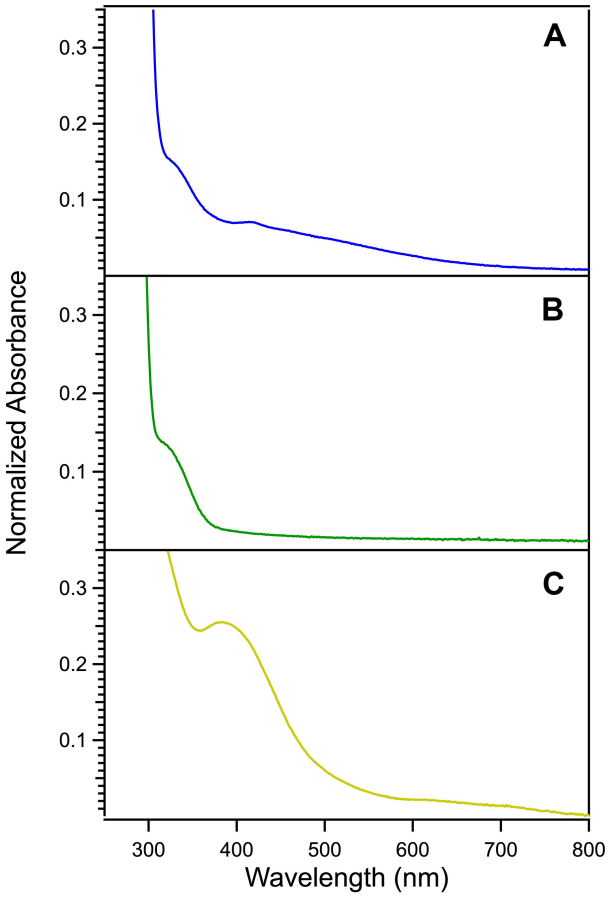
A
B
C
0.3
0.2
0.1
Normalized Absorbance
300
400
500
600
700
800
Wavelength (nm)

Figure 4.

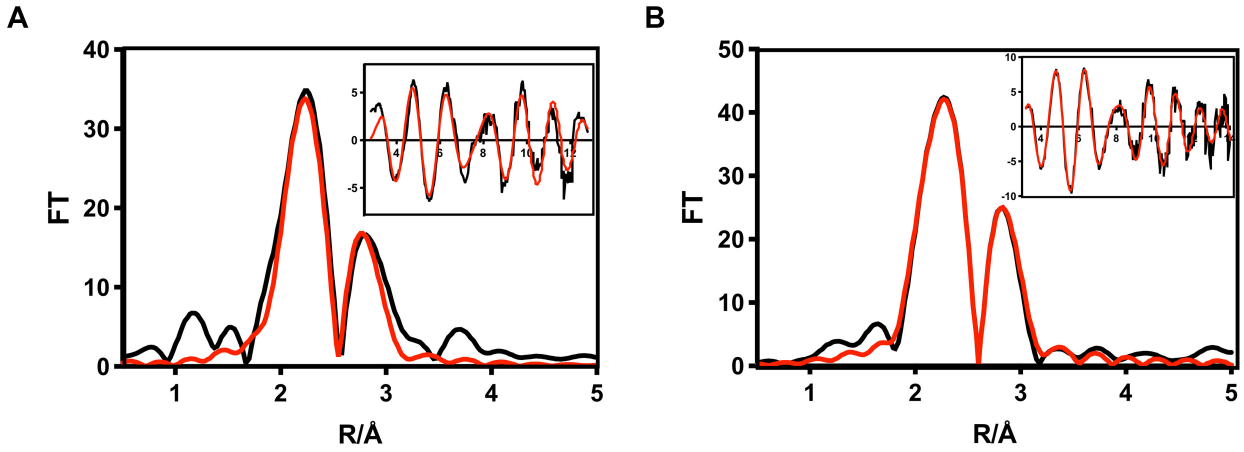

Figure 5.

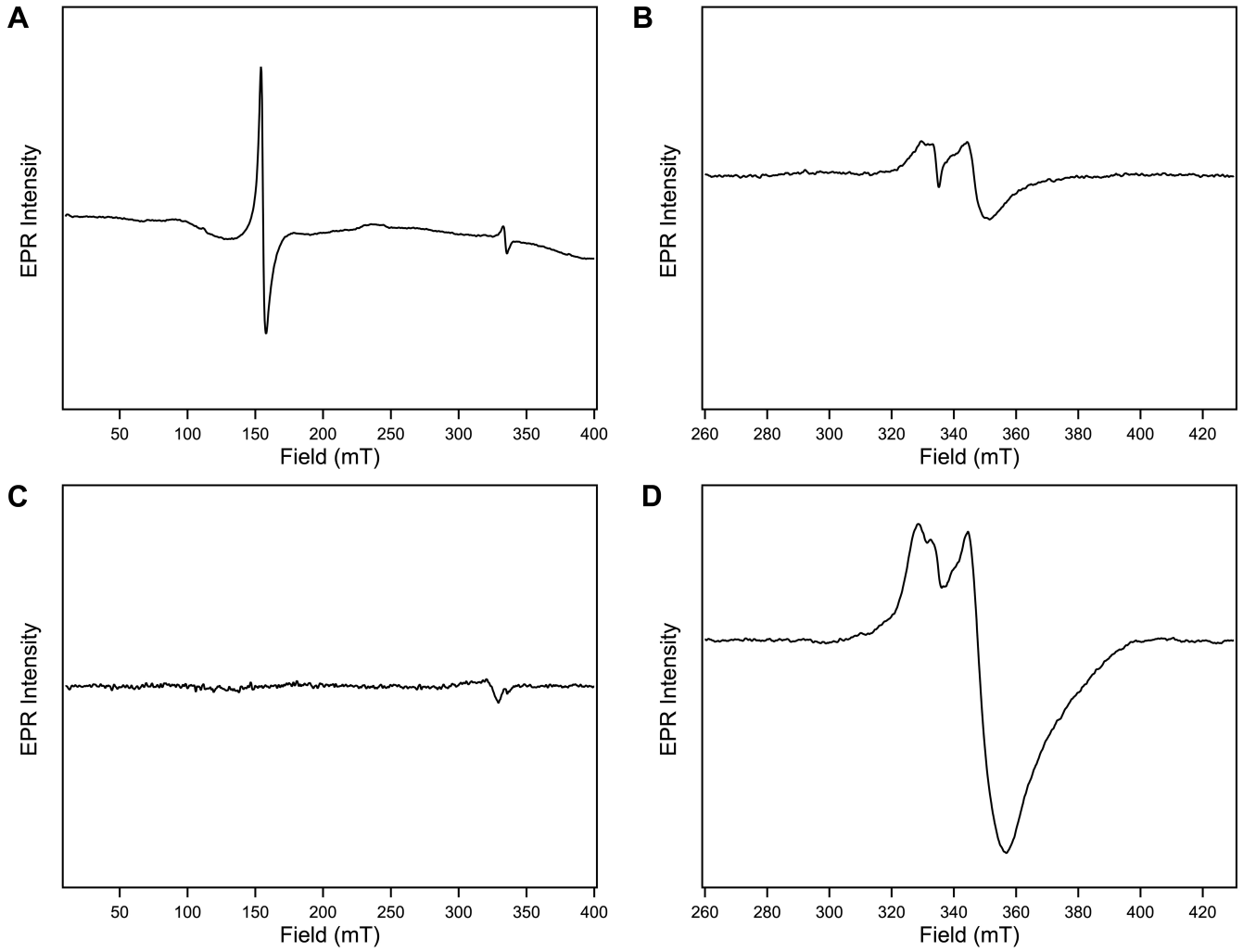
A
EPR Intensity
50
100
150
200
250
300
350
400
Field (mT)
B
EPR Intensity
260
280
300
320
340
360
380
400
420
Field (mT)
C
EPR Intensity
50
100
150
200
250
300
350
400
Field (mT)
D
EPR Intensity
260
280
300
320
340
360
380
400
420
Field (mT)

Figure 6.

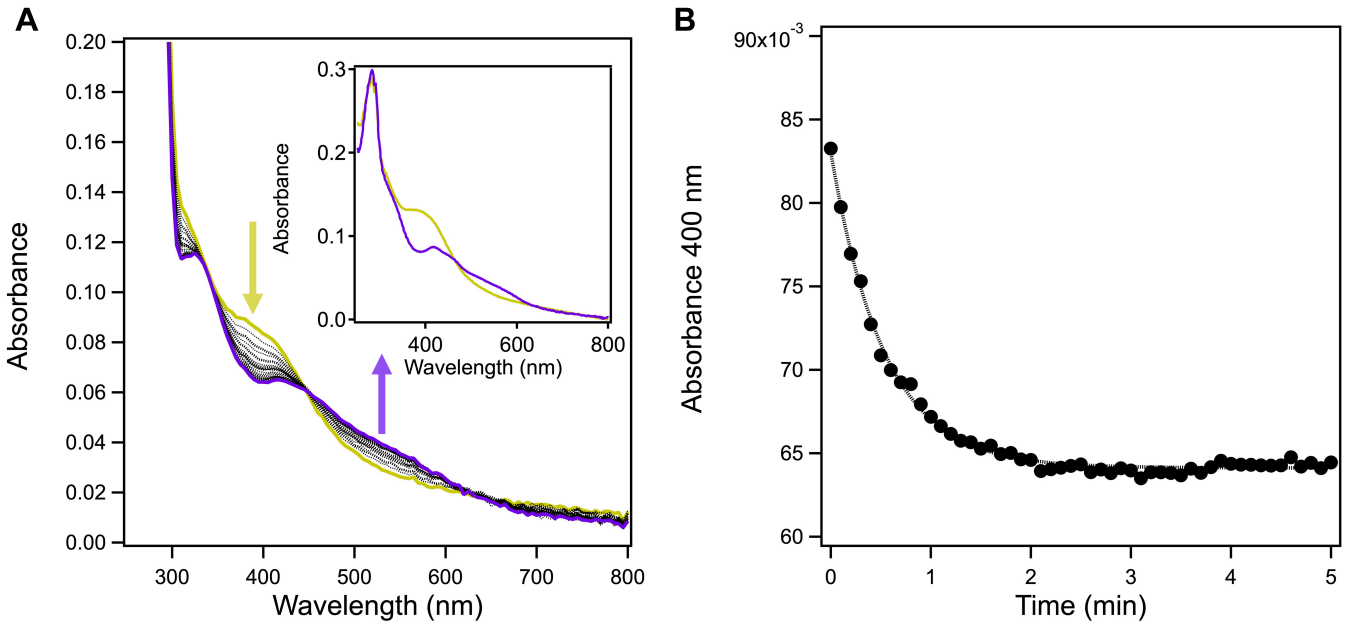
A
Absorbance
Wavelength (nm)
Absorbance
Wavelength (nm)
B
Absorbance 400 nm
90x10-3
Time (min)

Figure 7.

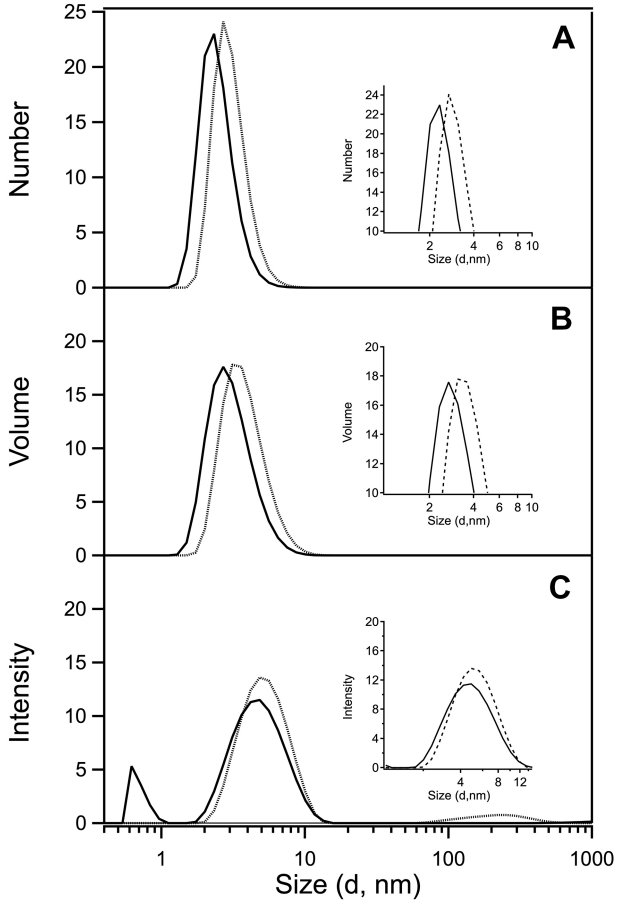

Figure 8.

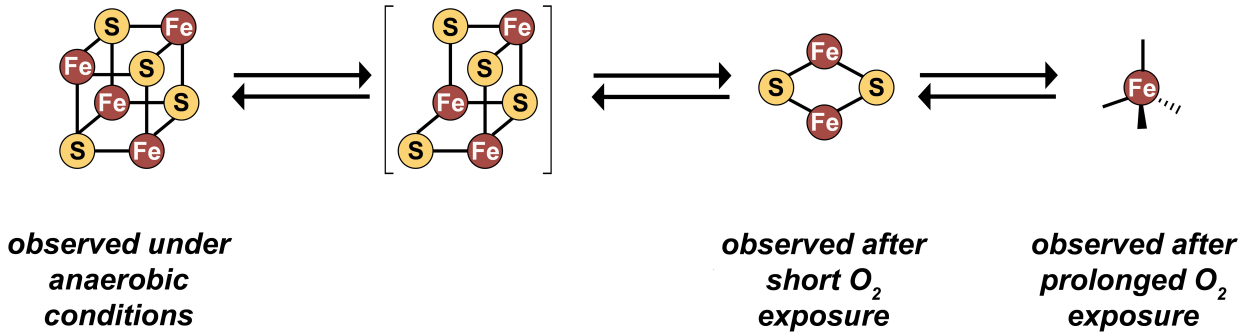
S
Fe
observed under anaerobic conditions
observed after short O_2 exposure
observed after prolonged O_2 exposure

For Table of Contents Only

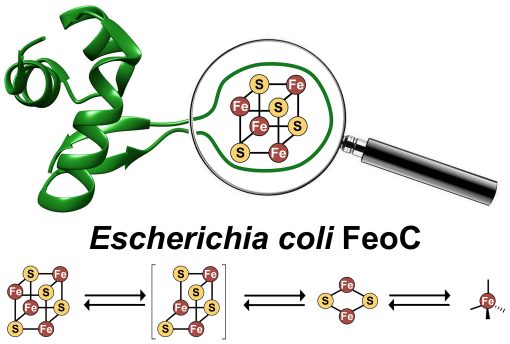

SUPPORTING INFORMATION

Escherichia coli FeoC binds a redox-active, rapidly oxygen-sensitive [4Fe-4S] cluster

Aaron T. Smith[1✉], Richard O. Linkous[1], Nathan J. Max[1], Alexandrea E. Sestok[1], Veronika A. Szalai[2], and Kelly N. Chacón[3]

[1]Department of Chemistry and Biochemistry, University of Maryland, Baltimore County, Baltimore, Maryland, 21250 USA

[2]Physical Measurement Laboratory, National Institute of Standards and Technology, Gaithersburg, Maryland, 20899, USA

[3]Department of Chemistry, Reed College, Portland, OR, 97202, USA

[✉]To whom correspondence should be addressed. Tel: 410-455-1985; E-mail: smitha@umbc.edu

Figure S1. The purification and cleavage of the MBP-*Ec*FeoC fusion. **A**. SDS-PAGE analysis (acrylamide mass fraction of 15 %) of the intact and cleaved forms of MBP-*Ec*FeoC. MW: molecular weight marker lane; lane 1: purified MBP-*Ec*FeoC fusion; lane 2: cleavage mixture of MBP-*Ec*FeoC after treatment with TEV protease; lanes 3-5: Superdex 75 SEC fractions; lane 6: empty; lane 7: final purified, concentrated cleaved *Ec*FeoC. **B**. Superdex 75 size-exclusion chromatogram of the cleavage mixture in panel **A**, lane 2. V: void volume; 3: panel **A**, lane 3 (protein aggregate); 4: panel **A**, lane 4 ($(His)_6$-MBP); 5: panel **A**, lane 5 (cleaved *Ec*FeoC prior to concentrating).

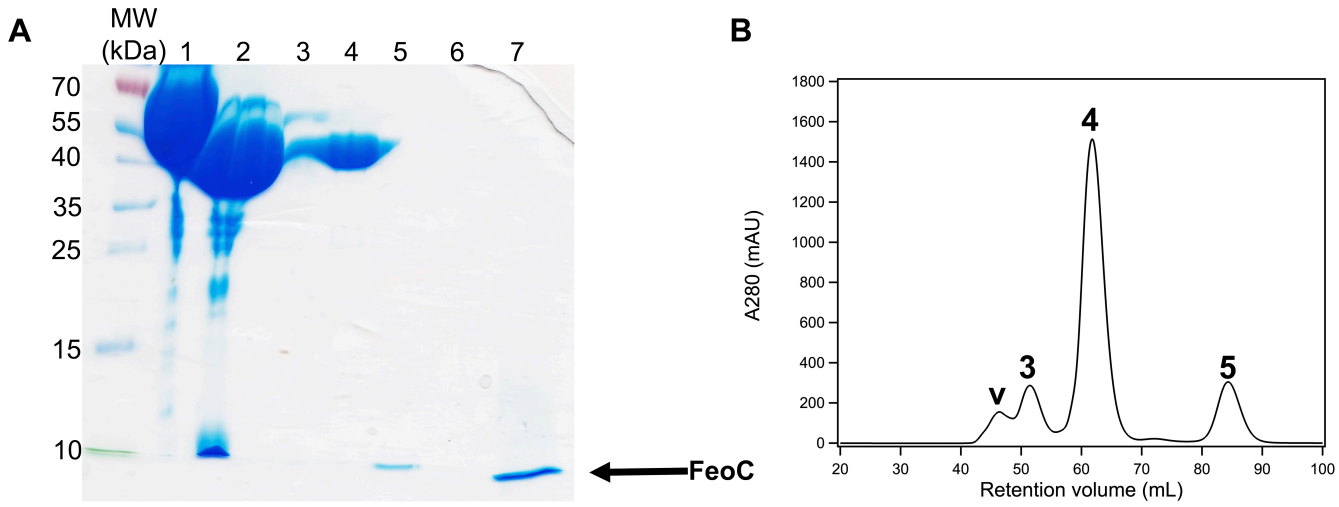

Figure S2. Far-UV circular dichroism spectrum of cleaved, apo *Ec*FeoC. Protein (0.1 mg/mL) was contained within in a UV-transparent quartz cuvette in phosphate-buffered saline (PBS; 0.137 mol/L NaCl, 0.0027 mol/L KCl, 0.01 mol/L Na_2HPO_4, 0.0018 mol/L KH_2PO_4, pH 7.4) at room temperature. The shown spectrum represents the average of 5 spectra.

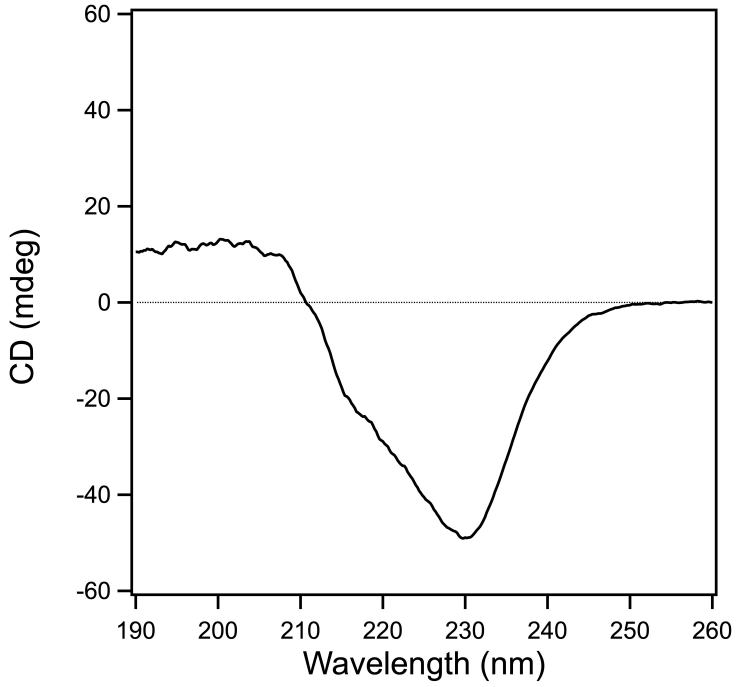

Figure S3. Electronic absorption spectra of as-isolated MBP-*Ec*FeoC prior (blue spectrum) and after (black spectrum) the addition of sodium dithionite. Samples were at room temperature in 25 mmol/L Tris buffer, pH 7.5, 200 mmol/L NaCl, 10 mmol/L maltose, and 0.7 mol/L glycerol (5 % (v/v) without (blue) or with (black) 1 mmol/L sodium dithionite.

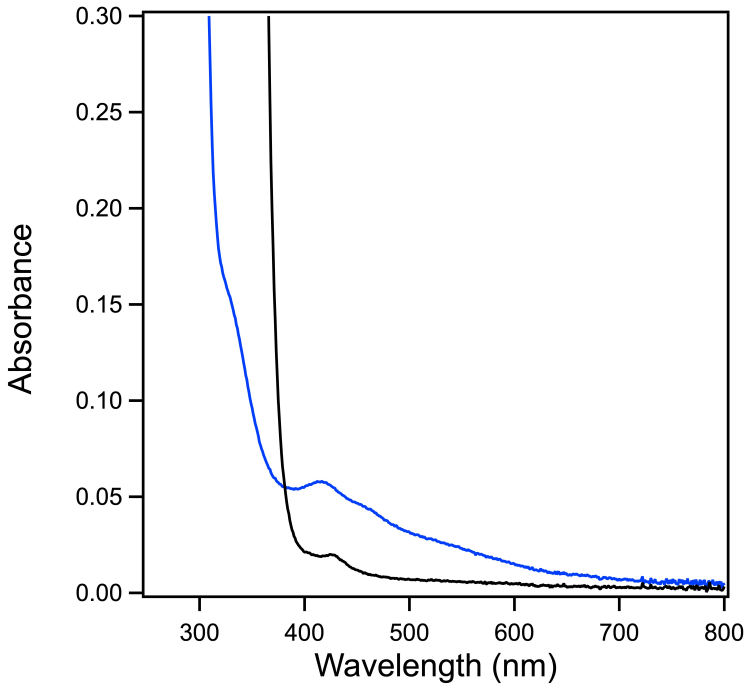

Figure S4. The $[4Fe\text{-}4S]^{2+}$ cluster of *Ec*FeoC is rapidly oxygen sensitive. **A**. Representative time course spectra of cleaved, anaerobically reconstituted *Ec*FeoC reacting upon the exposure to ambient atmosphere. Spectra were taken every 6 s (for clarity, only spectra every 30 s are displayed black and dotted) immediately after exposure of the previously anaerobic sample to air until reactivity stopped (≈ 15 min). The $[4Fe\text{-}4S]^{2+}$ spectral features (goldenrod) are rapidly lost and the appearance of the $[2Fe\text{-}2S]^{2+}$ spectral features rapidly appear (purple). The inset represents the plots of the two species before (goldenrod) and after (purple) reaction. The sample was in 50 mmol/L MOPS buffer, pH 7.5, 150 mmol/L NaCl, and 1 mmol/L DTT at room temperature. **B**. Representative plot of the kinetic decay of the absorbance feature at 400 nm (closed circles), characteristic of the $[4Fe\text{-}4S]^{2+}$ cluster. The presence of a lag phase (≈ 0 min to 6 min) and two separate kinetic phases (≈ 6min to 10 min and ≈ 10 to 14 min) are seen, but these may be due to the limited diffusion of O_2 into degassed buffer.

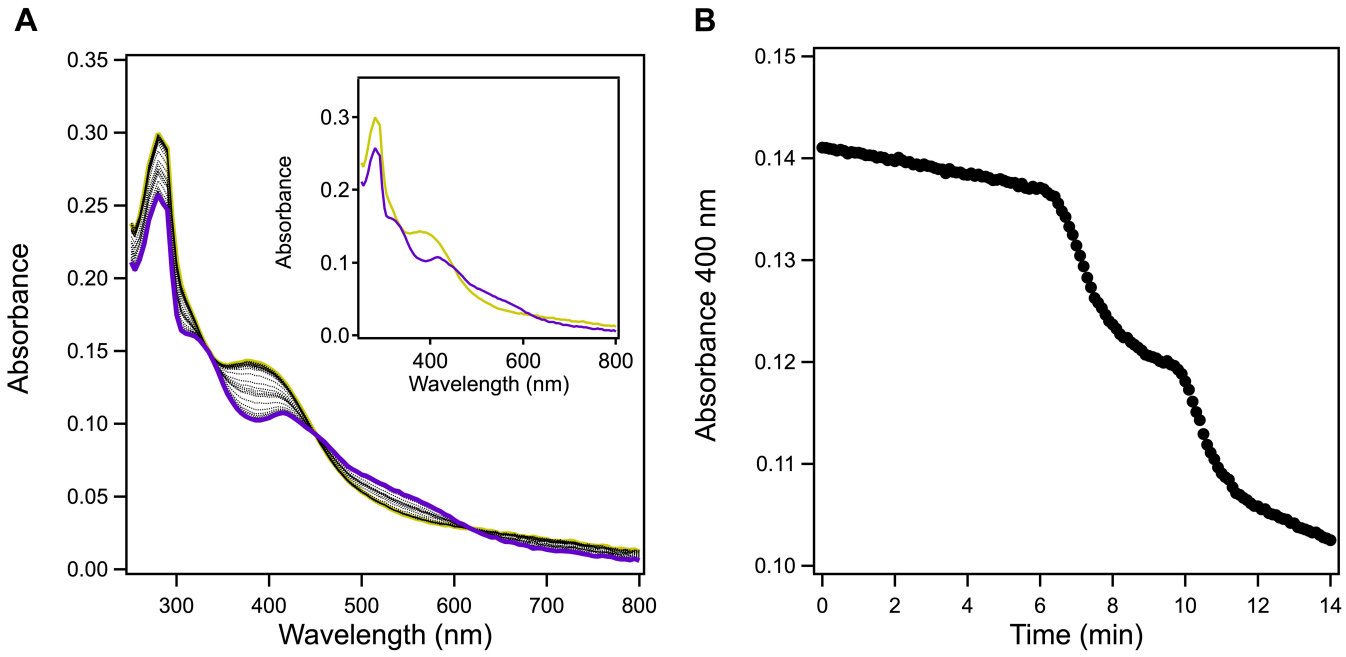

Figure S5. After oxidation of the $[4Fe\text{-}4S]^{2+}$ cluster to the $[2Fe\text{-}2S]^{2+}$ cluster and filtration, *Ec*FeoC remains monomeric (≈ 9000 g/mol, 9 kDa) based on its gel-filtration retention volume on Superdex 75.